



HAL
open science

Major modification of sediment routing by a large Mass Transport Deposit in the Gulf of Lions (Western Mediterranean)

B. Dennielou, Isabelle Jégou, Laurence Droz, Gwenael Jouet, Antonio Cattaneo, Serge S. Berné, Daniel Aslanian, Benoît Loubrieu, Marina Rabineau, Sylvain Bermell

► To cite this version:

B. Dennielou, Isabelle Jégou, Laurence Droz, Gwenael Jouet, Antonio Cattaneo, et al.. Major modification of sediment routing by a large Mass Transport Deposit in the Gulf of Lions (Western Mediterranean). *Marine Geology*, 2019, 411, pp.1-20. hal-02014178

HAL Id: hal-02014178

<https://hal.univ-brest.fr/hal-02014178v1>

Submitted on 21 Oct 2021

HAL is a multi-disciplinary open access archive for the deposit and dissemination of scientific research documents, whether they are published or not. The documents may come from teaching and research institutions in France or abroad, or from public or private research centers.

L'archive ouverte pluridisciplinaire **HAL**, est destinée au dépôt et à la diffusion de documents scientifiques de niveau recherche, publiés ou non, émanant des établissements d'enseignement et de recherche français ou étrangers, des laboratoires publics ou privés.



Distributed under a Creative Commons Attribution - NonCommercial 4.0 International License

1 **Major modification of sediment routing by a large Mass Transport Deposit in the**
2 **Gulf of Lions (Western Mediterranean)**

3

4 B. Dennielou¹, I. Jégou^{2,1}, L. Droz², G. Jouet¹, A. Cattaneo¹, S. Berné³, D. Aslanian¹, B.
5 Loubrieu¹, M. Rabineau², Sylvain Bermell¹

6

7 1- IFREMER, Centre de Brest, Unité de Recherche Géosciences Marines, 29280 Plouzané,
8 France

9 2- UMR 6538 Géosciences Océan, Université de Brest, UBO, Institut Universitaire
10 Européen de la Mer, France

11 3-Université de Perpignan, Laboratoire CEFREM, UMR-CNRS 5110, 52 Av. P. Alduy,
12 66860 Perpignan, France

13

14 **Keywords**

15 Gulf of Lions, Ebro margin, Sediment routing, Rhone deep-sea fan, Canyon, Mass
16 transport deposit, Turbidite

17

18 **Highlights**

19 - Submarine Mass Transport Deposits can radically modify sediment routing pathways
20 on the continental slope and rise.

21 - Large Mass Transport Deposits (160 km³) can be obscured on the seabed where
22 sedimentation rate is high.

23

24 **Abstract**

25

26 In the Gulf of Lions (Western Mediterranean), the emplacement of a large (160 km³)
27 Mass Transport Deposit, the Rhone Western Mass Transport Deposit (RWMTD), at the
28 base of slope, aside the Rhone deep-sea fan between 1800 and 2700 m water depth,
29 resulted in a major modification of the sediment routing by clogging a drainage network
30 and blocking at the base of slope sediments that were previously routed into the
31 Valencia channel and the Balearic abyssal plain. The RWMTD was sourced from
32 sediments of the western flank of the Rhone upper fan and the adjacent base of slope.
33 The mass transport deposit is characterized by a transparent seismic facies and
34 sediment cores show that it is composed of a stiff laminated muddy lithofacies
35 characteristic of the Rhone fan turbidites with marked contorted beds indicative of
36 remoulding. AMS radiocarbon dating shows that the RWMTD was emplaced between
37 19.9-21.5 ka cal. BP. It is coeval, within dating uncertainties, with the emplacement of a
38 megaturbidite in the Balearic Abyssal Plain and immediately predates a major avulsion
39 of the Rhone turbidite channel that led to the emplacement of an avulsion lobe (the
40 neofan) on top of the RWMTD. It is not possible to affirm a genetic link between these
41 three major gravity events but one can argue that they share a common forcing in
42 relation with massive turbiditic accumulation during the last sea-level lowstand at the
43 end of the Last Glacial Maximum. This study outlines the importance of mass transport
44 deposits in the building of turbidite systems and, more generally, the major control of
45 mass wasting on the routing and dispersal of sediments across continental margins.

46

47 **1. Introduction**

48

49 Besides geohazard and societal issues, slope failures and mass transport deposits play a
50 significant role in the long-term evolution of continental margins because they involve

51 the displacement of very important volumes of sediments and significantly modify the
52 margins morphology and the submarine sediment dispersal pattern (Huppertz et al.,
53 2010; Joanne et al., 2010; Kawamura et al., 2010; Mulder, 2011; Shipp et al., 2011).
54 Furthermore, mass transport deposits may represent up to 10-20% of stratigraphic
55 sequences on continental margins (McHugh et al., 1996; Mulder, 2011; Weimer, 1989).
56 They can play a significant role in the movement and transfer of sediment at river mouth
57 deltas or canyon heads at hourly or yearly time scales (Biscara et al., 2012; Clare et al.,
58 2016; Kelner et al., 2014; Mazières et al., 2014; Obelcz et al., 2017; Smith et al., 2007),
59 but also at geologic time scales on canyons and whole margin development (Micallef et
60 al., 2012; Sultan et al., 2007). This is particularly the case for large mass transport
61 deposits that instantaneously redistribute huge volumes of sediment, in the order of
62 several km³. These are dominantly emplaced on slopes receiving massive sediment
63 input such as glaciated margins (Bryn et al., 2005; Gales et al., 2014; Imbo et al., 2003;
64 Jansen et al., 1987; Lee, 2009; Piper et al., 2003) or deltaic margins during periods of low
65 sea level (Droz and Bellaiche, 1985; Garziglia et al., 2008; Nelson et al., 2011; Piper et al.,
66 1997; Weimer, 1989). They also represent a significant sediment input into abyssal
67 plains in the form of megabeds, particularly in the Mediterranean Sea (Cita and Aloisi,
68 2000; Reeder et al., 2000; Rothwell et al., 1998; San Pedro et al., 2017)}.

69 In the Gulf of Lions (GoL) (Western Mediterranean) (Fig. 1), the Rhone deep-sea fan
70 developed since the Pliocene in a complex geologic setting characterized by a
71 continental slope dissected by several shifting canyons (Berné et al., 1999; Bourcart,
72 1960; Torres et al., 1995), salt tectonics (dos Reis et al., 2005; Droz, 1983; Gaullier,
73 1993; Le Cann, 1987) and canyon and open slope mass wasting (Sultan et al., 2007).
74 Mass transport deposits on the Rhone fan have long been recognized as major features
75 with high impact on the Late Quaternary fan growth (Droz and Bellaiche, 1985; Gaullier

76 et al., 1998). We present a new detailed mapping of the superficial Rhone Western mass
77 transport deposit (RWMTD) based on a synthesis and reinterpretation of bathymetric
78 and seismic data acquired during several oceanographic campaigns since 1997, and new
79 litho-facies and chronological data from three sediment cores that penetrated the
80 deposits. In addition to considerations on the sedimentary source and trigger
81 mechanisms, the aim of this study is to outline the role played by the emplacement of
82 the RWMTD at the base of slope in the evolution of sediment routing patterns in the
83 western part of the GoL from the upper slope to the Balearic Abyssal Plain within the
84 context of sea-level fluctuations since the Last Glacial Maximum (LGM).

85

86 **2. Geological background**

87 **2.1. Sedimentary setting**

88 Following the reflooding of the basin, after a major sea level drop of the Mediterranean
89 Sea during the Messinian (1500 m according to Hsü et al. (1973)), 3 km of prograding
90 and aggrading sediments were deposited throughout the Plio-Quaternary to reach the
91 present day margin morphology (Leroux et al., 2014; Lofi et al., 2003). Following the
92 Mid-Pleistocene transition (1,250- 700 ka BP; (Clark et al., 2006)), sediment
93 accumulation on the GoL margin increased by two-fold as a result of the increased
94 magnitude of global sea-level changes (Leroux et al., 2017). During the Late Pleistocene,
95 the evolution of the margin and canyons was driven by sea-level fluctuations and
96 thermal subsidence, in the order of 250 m.Ma^{-1} , creating accommodation prone to the
97 deposition of sediments (Rabineau et al., 2006; Rabineau et al., 2014). During sea-level
98 falls thick forced-regressive sequences developed (Bassetti et al., 2008; Rabineau et al.,
99 2005; Rabineau et al., 1998; Tesson and Gensous, 1998; Torres et al., 1995) bounded on
100 the slope by condensed intervals, deposited during highstands (Sierro et al., 2009).

101 During this period of time the evolution of the deep GoL was also controlled by syn-
102 sedimentary salt tectonics. Gravitational gliding and spreading over the Messinian
103 detachment salt level (dos Reis et al., 2005) developed at the mid to lower slope with
104 basinward-dipping active and buried listric faults parallel to sub-parallel to the shelf
105 break (dos Reis et al., 2005) (Fig. 2).

106

107 **2.2. Sediment routing**

108 In the GoL the main source of sediment is the Rhône River (Pont et al., 2002). Through
109 geological times, sediment dispersal at the mouth of rivers was controlled by sea level
110 fluctuations and the synchronous migration of the shoreline. During periods of low sea
111 level (glacials), the seaward migration of the shoreline moved the sediment depocenters
112 onto to the outer shelf and a significant amount of sediment was routed into the
113 canyons, as evidenced by preserved marked sinuous incisions at some canyons (Baztan
114 et al., 2005; Mauffrey et al., 2015). Numerous canyons dissect the shelf break. In the
115 western part of the GoL, eight canyons, Cap de Creus to Marti canyons, coalesce down
116 slope but do not show a connection with the Valencia channel (Amblas et al., 2006;
117 Baztan et al., 2005; Berné et al., 2004). In the central adjacent part the Petit-Rhone
118 canyon shows a sinuous pattern and is prolonged by the Rhone turbidite system (Droz
119 et al., 2006) (Fig. 1). The developed sinuous channel network of the Rhone turbidite
120 system (Droz et al., 2006) shows that during lowstands a large amount of sediment was
121 efficiently exported as deep as 2800 m water depth and possibly into the Balearic
122 Abyssal Plain. To the west, the sediments were likely funneled into the Sète canyon
123 network and deposited at the base of slope where the canyons morphology abruptly
124 smoothens (Fig. 1). The same configuration applies for La Fonera and Clots del Puget
125 canyons. In comparison, to the southwest, on the south Catalan margin canyons coalesce

126 and extend beyond the base of slope to finally vanish into the Valencia Fan at the
127 northernmost part of the Algerian–Balearic Abyssal plain (Amblas et al., 2011;
128 Maldonado et al., 1985) (Fig. 1). One particularly noteworthy event during the last sea-
129 level rise on the Ebro margin was the emplacement of the Big'95 mass transport deposit
130 that caused a sudden change in sedimentation style in the upper segment of the Valencia
131 drainage network, with a significant decrease in sediment transport and incision
132 capacity (Amblas et al., 2011).

133

134 **2.3. Turbidite systems**

135 Two thick turbidite systems lie at the base of slope in the GoL, the Rhone turbidite
136 system in the central part of the GoL and the Pyreneo-Languedocian Sedimentary Ridge
137 to the west as shown on the Quaternary isopach map (dos Reis et al., 2005). Smaller
138 turbiditic sedimentary ridges lie at the right hand side of the La Fonera and Clots del
139 Puget canyons (Fig. 1). All these turbidite systems consist of terrigenous sediment,
140 starved during the Holocene highstand, and displaying high sedimentation rates during
141 the LGM lowstand (Beaudouin et al., 2004; Jallet and Giresse, 2005; Lombo Tombo et al.,
142 2015; Melki et al., 2009). The Rhone turbidite system, the largest turbidite system in
143 terms of thickness and area in the GoL and in the western Mediterranean Sea, lies in the
144 prolongation of the Petit-Rhône canyon that seems to have been the main feeder
145 throughout the Quaternary (Droz and Bellaiche, 1985). It represents an accumulation of
146 ca. 3,600 m of turbidites and mass-transport deposits. On the the upper fan, between
147 1,350 m and 2,000 m water depths, a perched valley, 12 to 4 km wide and 500 to 200 m
148 deep, is cut by a narrow, 1,000 to 600 m wide and 150 to 100 m deep, axial meandering
149 channel (Lombo Tombo et al., 2015; O'Connell et al., 1991; Torres et al., 1997) (Fig. 1).
150 The last channel avulsion most likely occurred during the LGM (Bonnell et al., 2005) and

151 led to the emplacement of a lobe-shaped fan, called neofan (Bonnell et al., 2005; Droz and
152 Bellaiche, 1985; Jégou, 2008; Torres et al., 1997)}. (Fig. 1).

153

154 **2.4 Slope instabilities**

155 At the base of slope numerous headwall scars are indicative of slope failures (Berné et
156 al., 2004; Droz and Bellaiche, 1985; Gaullier et al., 1998; Sultan et al., 2007; Torres et al.,
157 1995). Scars are superimposed on a network of buried and active listric faults parallel to
158 the margin (dos Reis et al., 2005; Torres et al., 1995) (Figs. 2). Although movements of
159 these faults driven by halokinesis may be a pre-conditioning factor or even a trigger
160 mechanism for sliding (Bellaiche et al., 1986; Droz, 1983) a causal link between these
161 features has not yet been shown. Two large mass transport deposits are lying on the
162 subsurface of the eastern and western sides of the fan and were named the Eastern and
163 Western (superficial) Transparent Series (Bellaiche et al., 1986; Droz and Bellaiche,
164 1985), Intermediate Unit (Gaullier et al., 1998), Middle Unit (Méar and Gensous, 1993),
165 Eastern and Western Debris Flow (Bonnell et al., 2005; Droz et al., 2001; Lastras et al.,
166 2007a) and more recently Western and Eastern Mass Transport Deposits (WMTD and
167 EMTD) (Droz et al., 2006). In this paper we will adopt the Rhone Western and Eastern
168 Mass Transport Deposits (RWMTD and REMTD) nomenclature. These mass transport
169 deposits are characterized by transparent seismic facies with no apparent internal
170 structures apart from some undisturbed tilted block in the proximal area (Droz and
171 Bellaiche, 1985). Concave and undulated features on top of both deposits, at the contact
172 with adjacent undisturbed strata were interpreted as compression ridges formed by
173 displaced material at the toe of the slope (Droz and Bellaiche, 1985). Scars surrounding
174 both deposits are visible on the fan levees and on the adjacent base of slope suggesting
175 that sliding has affected the whole base of slope and upfan area (Gaullier et al., 1998).

176 The age of these mass transport deposits remains speculative due to the lack of direct
177 dating. Seismic stratigraphy and coring showed that both are covered by a metric
178 pelagic drape and that the RWMTD is overlapped by the neofan deposits (Bonnell et al.,
179 2005; Droz and Bellaiche, 1985; Gaullier et al., 1998; Torres et al., 1997; Torres et al.,
180 1995) showing that turbiditic activity persisted after its emplacement, This suggests
181 that both deposits probably emplaced during the Last Glacial Maximum, but close to the
182 post-glacial sediment starvation of the Rhone fan dated at ca. 18.5 ka cal BP (Beaudouin
183 et al., 2004; Dennielou et al., 2006; Lombo Tombo et al., 2015).

184

185 **3. Data and methods**

186 This study is based on a variety of bathymetry and seismic data collected since 1997
187 during several oceanographic campaigns (Fig. 3; Tab. 1) as well as on three piston cores
188 (Tab. 2).

189 Two bathymetric Digital Terrain Models (DTMs) were used: a 500 m resolution DTM
190 (IFREMER/CIESM, 2011) and unpublished 50 m and 100 m resolution DTMs based on
191 Simrad EM12 and EM300 multibeam surveys during oceanic campaigns listed (Tab. 1).

192 Detailed mapping of the RWMTD is based on various seismic data including single and
193 multi-channel GI and mini-GI (vertical resolution in the order of 30 and 10 m,
194 respectively) High Resolution (HR) sparker lines as well as Very High Resolution (VHR)
195 Sub-Bottom Profiler (SBP) lines (vertical resolution ca. 1 m) (Figs. 2, 3 and 4A; Tab. 1).

196 This dense and multi-resolution seismic database allowed a detailed new mapping and
197 characterization of the RWMTD and to produce isochore and isochron maps.

198 Two sediment cores were collected with the giant Calypso piston corer aboard R/V
199 Marion Dufresne on the northern and southern extremities of the RWMTD. Another core
200 was collected in the central part of the RWMTD with a Kullenberg piston corer aboard

201 R/V Le Suroit (Figs. 2, 3 and 4A; Tabs. 1 and 2). Identification of lithofacies and grain
202 size is based on visual description and physical properties logging with a Geotek Multi-
203 Sensor Core Logger. AMS radiocarbon dating was conducted on monospecific planktonic
204 foraminifera (*Globigerina bulloides*). Age calibration into calendar scales was calculated
205 by Calib 7.1 software (Stuiver et al., 2018) with the marine13 calibration curve (Reimer
206 et al., 2013).

207 All data were integrated into the IHS Kingdom suite seismic interpretation software. For
208 the interpolation of isochrone and isochore grid, we used the Flex Gridding algorithms,
209 defining a cell size of 50 m. Conversion of seismic two-way travel times into meters in
210 the sedimentary column was made with a sound velocity of 1600 m.s⁻¹, which may
211 represent the minimum sound velocity according to wave velocities measured in
212 sediment cores.

213

214 **4. Results**

215 **4.1 Seabed morphology**

216 The RWTMD has a faint expression on the seabed (Fig. 1) because it is partly overlain by
217 more recent deposits that are the Rhone Neofan, the Pyreneo-Languedocian Sedimentary
218 Ridge (Berné et al., 1999) and some deposits at the outlet of La Fonera canyon (Droz et
219 al., 2001). The seabed morphology is also imprinted by erosional scours developed
220 during the lowstand functioning of the Neofan (Bonnell et al., 2005) and of Cap de Creus
221 canyon (Lastras et al., 2007b) which are still likely active due to deep water active
222 hydro-sedimentary processes related to open-ocean convection (Stabholz et al., 2013).

223 The most obvious morphological evidence of mass wasting lies in the occurrence of slide
224 scars in the proximal area of the RWMTD at the base of slope and on the side of the
225 Rhone fan (Fig. 4B). All scars show a NE-SW orientation. The orientation of the biggest

226 scar, 30 km long, 10-100 m high headwall, running along slope and gradually becoming
227 perpendicular to the slope on the side of Rhone fan between 2,000-1,900 m water depth,
228 suggests a relation with the RWMTD (Fig. 4B). To the SW the headwall is nearly parallel
229 to the slope at 2,100-2,200 m water depth, while to the NE it gradually becomes
230 perpendicular to the slope between 2,000-1,900 m water depth, on the side of Rhone fan
231 (Fig. 4B). Similar parallel headwalls, also facing to the SE, but shorter and discontinuous
232 and less high are visible about 4 km upslope to the north (Fig. 4B). About 4 km to the
233 south, on the side of the Rhone fan, a 15 km long headwall facing to the NW is
234 perpendicular to the slope (Fig. 4B). The configuration of headwalls across the side of
235 the Rhone fan forms a 7 km wide, 40 m deep along slope corridor that can be
236 interpreted as a pathway for the RWMTD. Noteworthy, the scars are superimposed to
237 the active and buried listric faults network developed by syn-sedimentary salt tectonics
238 (dos Reis et al., 2005) (Fig. 4B).

239 To the south, the only obvious morphological expression of the RWMTD is a faint NE-SW
240 lineation at the foot of a Rhone fan channel-levee and corresponding to a compression
241 bulge at the lateral toe contact between the RWMTD and the Rhone fan (Fig. 4C).

242

243 **4.2 Seismic structure of the RWMTD and of adjacent and underlying sediments**

244 The RWMTD appears as a body with a transparent acoustic facies on the VHR, low
245 penetration, SBP lines and on the HR single channel seismic lines (Figs. 5 to 9). However,
246 on the 24-channel HR seismic it shows sub-continuous internal reflections roughly
247 parallel to the seabed that onlap on the sedimentary basement (Fig. 5B). This is evidence
248 that the infill occurred on an inherited morphology. In some areas the top reflector,
249 close to the seabed, shows incisions and roughness, but in relation to more recent
250 superficial deposits or hydro-sedimentary processes such as the neofan channels and

251 scours (Figs 6B, 7 and 8). Truncation of the Rhone fan strata (Fig. 5C) indicates that the
252 RWMTD is related to the failure of the fan levee as also suggested by the collapsed
253 western levee of the Rhone fan. (Fig. 4B).

254 The top of the RWMTD is rather smooth and shows a slope towards the SW and towards
255 the south that roughly follows the overall trend of the underlying substratum (Fig. 10).
256 To the north and to the south, the RWMTD outcrops, at least at the seismic vertical
257 resolution, while in its central area it is overlapped to the east by the neofan deposits
258 (Figs. 5D and 10A) and to the west by a thin veneer of Pyreneo-Langudocian
259 Sedimentary Ridge deposits and of La Fonera canyon deposits (Fig. 5D, 7 and 8A). The
260 compression bulge to the SE in the distal area is clearly visible and clearly shows that
261 the RWMTD has overlapped the Rhone fan (Fig. 9).

262 On the VHR SBP lines the structure of the basement of the RWMTD is not visible because
263 of the low seismic penetration. On VHR seismic, in the proximal (north) area the
264 basement corresponds to stratified folded and/or faulted sediments characteristics of
265 the base of slope deposits to the north (Fig. 5D) and Rhone fan stratified Pleistocene
266 deposits to the east (Fig. 5). In the central area the RWMTD is confined between the
267 Rhone fan deposits, to the east, where it pinches out, and the stratified deposits of the
268 Pyreneo-Langudocian Sedimentary Ridge to the west (Figs. 6, 7, 8B and 9). From north
269 to south the RWMTD width is ca. 40 km in the proximal area, 50 km in the central area
270 and gradually narrows to 5 km in the most distal area. The horizontal run-out distance
271 (L) is 180 km (Fig. 10), the height fall (H), i-e the height between the head scar and the
272 most distal deposits is ca. 740 m and the H/L ratio is 0.004.

273

274 **4.3 Extension, thickness and morphology at the base of the RWMTD**

275 The RWMTD extends from 1,900 to 2,700 m water depth and covers a surface of 6800
276 km². The isochrones map of the basement shows that the RWMTD is emplaced in the
277 large depression between the Rhone fan and the Catalan margin (Fig. 10B). The
278 thickness of the RWMTD (Fig. 10C) is largely between 10 and 50 m thick, with the
279 thickest deposits (67 m) located along a large valley against the Rhone fan (Fig. 10C).
280 Otherwise, downslope, the thickness is rather constant and the volume of the RWMTD is
281 estimated at 160 km³. By comparison earlier mapping with low resolution seismic gave
282 a surface of ca. 7500 km² with a thickness up to 120 mstwt (96 m) and commonly
283 around 50 mstwt (40 m) for an estimated volume of 230 km³ (calculation after Gaullier
284 et al. (1998) with the same velocities as this study). For further comparison, the REMTD
285 covers an area of 7800 km² with a thickness up to 160 mstwt (128 m) and commonly
286 around 50-100 mstwt (40-80 m) for an estimated volume of 170 km³ (Coutellier, 1985;
287 Droz and Bellaiche, 1985)

288 The morphology at the base of the RWMTD is very different from the present-day
289 seabed. Besides an overall slope gradient to the SW and south, it shows a complex
290 morphology characterized by highs and lows. To the north the most proximal deposits
291 lie on stair-like morphologies corresponding to the tip of listric faults (Fig. 5D). To the
292 east, the contact with the adjacent Rhone fan is characterized by truncations of the fan
293 levees indicative of failure and collapse of the levee (Fig. 5C). To the south the RWMTD
294 fills several depressions that build a 12 to 18 km wide and 30 m deep valley against the
295 Rhone fan (Figs 5C, 7 and 9) in the continuation of the present Sète canyon outlet,
296 widening downslope and that connects to the Valencia valley. The RWMTD shows a
297 bifurcation to the SW where it becomes narrower (5 km) and connects to the Clots del
298 Puget and Valencia valleys (Figs. 8C and 8D). A parallel but fainter valley also runs along
299 the Pyreneo-Languedocian Sedimentary Ridge (Fig. 10B). This buried valley to the east

300 shows a concave-up longitudinal profile that fits with the concave-up longitudinal shape
301 of the Sète canyon and Valencia channel suggesting that the three valleys were a
302 continuum before the emplacement of the RWMTD (Fig. 10D).

303

304 **4.4 Lithofacies and chronology of the RWMTD**

305 Three sediment cores were collected in areas where the RWMTD outcrops at the seabed
306 at the seismic resolution. Core MD01-2435 was collected at a RWMTD proximal location
307 where the WMTD lies on the Rhone fan deposits (Fig. 6A), core KSGC-10 was collected at
308 a RWMTD central location on the neofan area where scours have eroded into the
309 RWMTD and open-ocean convection has prevented the deposition of sediment since
310 beginning of the Holocene (Denniellou et al., 2009; Stabholz et al., 2013), core MD01-
311 2438 was collected at a RWMTD distal location (Figs. 2, 3 and 6B). Sediment in MD01
312 cores show disturbance related to non-stationary behaviour of the piston, which led to
313 oversampling during coring (Bourillet et al., 2007; Skinner and McCave, 2003), thus
314 preventing straightforward correlation between cores and seismic data. However, the
315 identification of lithofacies was still possible, and sharp contrasts between pelagic,
316 turbiditic and mass transport deposits make straightforward the analogy between
317 lithofacies and well-contrasted seismic facies.

318 Three sedimentary units were identified (Fig. 11). Unit 1 is composed of foraminifera
319 and calcareous nannoplankton oozes that correspond to ambient pelagic sedimentation.
320 Unit 2 is composed of laminated mud with frequent silt to very fine sand laminae. This
321 facies is interpreted as turbidites deposited by turbidity current spillover from the
322 adjacent perched valley. They are similar to those already described in the Rhone fan
323 valley or on the neofan levees (Bonnell et al., 2005; Denniellou et al., 2006; Lombo Tombo
324 et al., 2015). Unit 3 is composed of stiff mud with colour banding corresponding to

325 sulphide rich laminae and few silt layers characteristics of lithofacies in the Rhone fan
326 (Lombo Tombo et al., 2015). Laminae are either horizontal, oblique or show tight
327 folding. In core MD01-2438 a layer of coarse material in the form of fine to very coarse
328 sand bioclasts and lithoclasts have been involved in the sediment deformation but no
329 evidence of matrix supported clasts or blocks was found. This lithofacies is much denser
330 ($>2 \text{ g.cm}^{-3}$) and stiffer than the units above with similar (muddy) grain sizes (Fig. 11)
331 suggesting that it is over-consolidated and was therefore either previously buried
332 deeper than its present stratigraphic depth or has gained strength after remoulding. The
333 unit is interpreted as the RWMTD deposits. The plastic deformation and contortion are
334 indicative of shearing and the lack of faulting and blocks show that the sediment
335 remained a coherent mass, at least for the upper sampled part, so that the RWMTD can
336 be classified as a slide or slump because of evidence of plastic deformation (cf. Mulder
337 and Cochonat (1996); Piper et al. (1997); Tripsanas et al. (2008); Nelson et al. (2011);
338 Shanmugam (2015)). The transparent echo-facies that characterizes the RWMTD is
339 commonly interpreted as indicative of disintegration as a result of break up of blocks in
340 the downslope evolution of a slide into a debris flow (Piper et al. 1997). The absence of
341 blocks in the retrieved sediment cores may be due to the low penetration. However, the
342 sediment contortion is also a factor of strata disorganisation consistent with the
343 transparent echo-facies.

344 In core MD01-2435 (Fig. 11) Unit 1 is described from top to 0.25 m and Unit 2 from 0.25
345 to 8.90 m. The contact between the units is oblique and erosional. Unit 3 is described
346 from 8.90 to 15,50 m, colour banding is horizontal to sub-horizontal (up to 15°
347 inclination) but inclination varies down core. From 15.50 m to the base of core, the
348 sediment is fully disturbed because it was sucked up during coring, however, despite
349 disturbance the collected sediment is very similar to Unit 3.

350 In core KSGC-10 (Fig. 11), only Unit 3 is present showing that no sediments were
351 deposited during the Holocene (Denniellou et al., 2009; Stabholz et al., 2013).

352 In core MD01-2438 (Fig. 11) Unit 1 is described from 0 to 1.00 m. Two layers of coarse
353 sand (2 and 16 cm thick) are intercalated in the unit and correspond to post-glacial and
354 Holocene turbidites already described at the base of slope of the study area (Denniellou
355 et al., 2009). Unit 2 is not present and Unit 1 rests on Unit 3. Unit 3 is described from
356 1.00 m to the base of core (8.00 m), the contact between Unit 1 and 3 is sharp and
357 horizontal. Colour banding is contorted from 1.00 m to 5.00 m and becomes gradually
358 horizontal to sub-horizontal downcore. From 8.00 m to the base of core the sediment is
359 also fully disturbed and the collected sediment is very similar to Unit 3.

360 Radiocarbon dating (Tab. 3 and Fig. 11) shows that the hemipelagic Unit 1 was
361 deposited during the deglacial sea level rise and during the Holocene highstand and that
362 turbiditic Unit 2 was deposited at the end of the LGM during and shortly after the onset
363 of the sea level rise (20.7-14.7 ka cal BP). These ages are consistent with those obtained
364 for the same units on the Rhone fan and adjacent areas (Beaudouin et al., 2004; Bonnel
365 et al., 2005; Dennielou et al., 2006; Dennielou et al., 2009; Lombo Tombo et al., 2015).
366 Ages obtained at the top of the RWMTD (Unit 3) and at the base of overlapping units
367 (turbiditic Unit 2 in the proximal position and Unit 1 in the distal position) are similar
368 and show that emplacement of the RWMTD occurred between 19.9 and 21.5 ka cal BP (2
369 sigma) with an average median age of 21.0 ka cal BP (Fig. 12). However, this does not
370 discard a possibility of several stages of sliding in this age bracket.

371

372 **5. Discussion**

373 **5.1. The Rhone WMTD: a hidden landslide**

374 Unlike several recent mass transport deposits around the world (e.g. Storegga (Bugge et
375 al., 1988), BIG'95 (Lastras et al., 2002), Ruatoria (Collot et al., 2001), among the largest),
376 the RWMTD has a faint seabed morphological expression and could be easily overlooked
377 if no seismic data was available. The lack of morphologic expression is a consequence of
378 two factors : (1) the fact that displaced and deposited sediment infilled the topographic
379 low between the Rhone fan and Pyreneo-Languedocian Sedimentary Ridge and adjacent
380 slope to the west (Fig. 1) and did not created any distal positive relief, (2) seabed
381 rejuvenation by rapid burying related the high sedimentation rates that persisted at the
382 base of slope until 18.5 ka BP (Bonnell et al., 2005; Lombo Tombo et al., 2015), i-e during
383 ca. 1.5 to 3.5 ka after the emplacement of the RWMTDT, and by the development of the
384 neofan avulsion lobe and channel-levee on top of it.

385 At river mouth subaqueous deltas or upper slopes under high sedimentation rates
386 sliding seems to be a frequent quasi intrinsic process of sediment movement and
387 transfer but resulting morphologies are quickly buried and obscured, sometimes within
388 days to years (Biscara et al., 2012; Clare et al., 2016 ; Kelner et al., 2014; Mazières et al.,
389 2014; Obelcz et al., 2017; Smith et al., 2007). Our study shows that obscuration may
390 occur on much larger areas at slope bases. Indeed, the RWMTD case may be atypical but
391 it raises the question of the recognition of large mass transport deposits and outlines
392 that bathymetric data alone are not sufficient for their recognition on high
393 sedimentation rate continental margins such as glacigenic and deltaic margins and that
394 inventories (e.g. Urgeles and Camerlenghi, (2013)) may be incomplete at the largest end
395 of the spectrum.

396

397 **5.2. Source and trigger mechanisms**

398 The recurrence of mass transport deposits in many deep-sea fans on deltaic margins
399 such as the Mississippi (Twichell et al., 1991; Weimer, 1989), Amazon (Piper et al.,
400 1997), Danube (Popescu et al., 2001) or Nile (Garziglia et al., 2008) shows that sediment
401 loading, mostly during lowstands, is a major preconditioning factor for sliding. Sliding
402 can occur when the stress exceeds the sediment strength and no external trigger
403 mechanism is actually needed to explain sliding of high sedimentation rate poorly-
404 consolidated sediment, even with low slopes, (Croguennec et al., 2017; Dennielou et al.,
405 2017). This configuration can be clearly invoked for the Rhone slope and fan where high
406 sedimentation rates, in the order of several meters per thousand years, during the Last
407 Glacial Maximum (Lombo Tombo et al., 2015; Sierro et al., 2009) have shortly preceded
408 the emplacement of the RWMTD. Among preconditioning factors, the occurrence of a
409 presently buried valley adjacent to the Rhone fan, in the continuation of the Sète valley,
410 suggests oversteepening by lateral retrogressive erosion along the Rhone fan. This
411 process has been proposed for explaining the broadening of the Bourcart Canyon
412 (Baztan et al., 2005; Sultan et al., 2007). At some stage, these recurrent failures may
413 have triggered a massive retrogressive failure of the fan levee and adjacent slope.
414 Another preconditioning factor could be local slope oversteepening by vertical
415 movements of listric faults (dos Reis et al., 2005) (Fig. 4B).

416 External triggers can occur and hasten sliding. In the GoL, earthquake shaking can be
417 discarded as the GoL is a low seismicity area where during the last 50 years most
418 earthquake magnitudes were lower than 4 (Manchuel et al., 2017). Furthermore, a
419 minimum magnitude of 7 is needed to trigger instabilities on high sedimentation rate
420 lowstand sediments in the neighbouring Bourcart Canyon (Sultan et al., 2007).

421

422 **5.3. Processes for propagation and long runout distance**

423 The RWMTD appears as a seismically homogenous and transparent body with no
424 evidence of particular internal structure. A large part of the body is buried under late
425 and post-glacial turbiditic deposits and erosions that might have obliterated
426 morphological features on top of the RWMTD (Bonnell et al., 2005; Droz and Bellaiche,
427 1985; Gaullier et al., 1998; Torres et al., 1997). However, seismic data reveal a rather flat
428 morphology on top (Figs. 6 to 10) and do not show evidence of faulting, blocks
429 formation, rafting or retrogression as observed in the neighbouring Big'95 landslide on
430 the Ebro Margin (Lastras et al., 2002; Lastras et al., 2004). On the contrary, the RWMTD
431 shows evidence of widespread ductile-plastic behaviour with folding and contortion in
432 the clay-rich sampled sediment (Fig. 11), and the formation of a compression bulge at
433 the SE limit against the Rhone fan (Figs. 4C, 4D and 9). The ductile-plastic interpretation
434 is reinforced by the fact that the RWMTD has spread onto and filled the pre-existing
435 seabed morphologies (Figs. 5 to 10).

436 Mass transport deposits can propagate over very long distances, in the order of several
437 hundreds of kilometres for the largests, and the runout distance is roughly proportional
438 to the size of the slide (De Blasio and Elverhøi, 2011; Haflidason et al., 2005). The
439 RWMTD exhibits a H/L ratio in the order of 0.004, which fits within the morphometric
440 characteristics of many mass transport deposits in the world (Issler et al., 2005). In
441 particular, it fits particularly well with the characteristics of the Storegga's 63 slide lobes
442 (Haflidason et al., 2005; Issler et al., 2005) suggesting that they share common
443 mechanical properties and propagation processes. Indeed, like the Storrega slide, the
444 RWMTD involved clay-rich sediments but with drastically different sources because the
445 Norwegian margin is fed by glacial and glacial sediments, while the GoL is fed by
446 temperate deltaic sediments. Many studies outline a discrepancy between the
447 mechanical properties (high strength, high density, low porosity) of cohesive sediment

448 in mass transport deposits and their exceptional long runout distances that would
449 necessitate much lower sediment strength (De Blasio et al., 2005). This is also the case
450 for the RWMTD that exhibits clay-rich sediments with exceptional high densities
451 (between 2 and 2.2 g.cm⁻³) that evidence over-consolidation with regards to the
452 overlying sediment (Fig. 11). Modelling of long runout distance by viscoplastic model
453 requires to introduce very low sediment strength (De Blasio et al., 2005), much lower
454 than that of the slided sediment and of the mass transport deposit. However,
455 remoulding of sediment and adjunction of water (shear wetting) during transport can
456 significantly decrease the sediment strength (De Blasio et al., 2005) and enhance
457 lubrication at the base and front of the mass transport deposit and explain long runout
458 distances (De Blasio and Elverhøi, 2011). In addition, hydroplaning may also increase
459 lubrication (De Blasio et al., 2005; Mohrig et al., 1998). The present high density of the
460 RWMTD suggests a drastic strengthening of sediment during transport or after
461 transport. Sediment densification is a common feature of mass transport deposits that
462 occurs in response of shearing in highly sensitive clays and explaining that they exhibit
463 contrasted impedance with the surrounding sediment and are very well imaged on
464 seismic data (Dugan, 2012). The important folding and contortion in the clay sediment
465 sampled on the top 7 m of the RWMTD at proximal, central and distal locations, is an
466 evidence that shearing occurred during transport and may thus explain the present high
467 density.

468

469 **5.4. Timing and synchronism with other major sediment gravity deposits in the** 470 **north-western Mediterranean**

471 The emplacement of the RWMTD is dated during the LGM between 19.9-21.5 ka cal BP
472 (end of the LGM) according to our radiocarbon dating at the base of sediment drape on

473 top of the RWMTD (Fig. 11). In the north-western Mediterranean, this period of time and
474 the ensuing post-glacial sea level rise are characterized by several other major events
475 that are the BIG'95 mass transport deposit (26 km³) on the Catalan-Ebro margin
476 (Lastras et al. 2002), the Rhone EMTD (150-200 km³) (Droz and Bellaiche, 1985; Droz et
477 al. 2006) in the GoL, and the megaturbidite in the Balearic Abyssal Plain (ca. 500 km³)
478 (Rothwell et al., 1998).

479 The BIG'95, seems to have been emplaced in a different setting than that of the RWMTD.
480 It affected the Ebro fed clay-rich deposits but that, unlike the Rhone fed deposits, are
481 less focused and spread through several canyons and developed at the base-of-slope
482 several channel–levee complexes with an apron-ramp turbidite system (Alonso and
483 Maldonado, 1990; Lastras et al., 2004). Sliding and long runout occurred at shallower
484 water depth from the upper slope at 200 m water depth to 2000 m water depth (and
485 more recently, at the end of the deglacial sea level rise at 11.0-11.5 ka cal BP (Lastras et
486 al., 2002; Lastras et al., 2004). However, like for the RWMTD, high sediment load and
487 over-steepening during lowstand may have been a determinant trigger mechanism
488 (Lastras et al., 2004).

489 The age of the REMTD is still unknown but like the RWMTD it is very shallow, it also
490 involved adjacent turbidite leveed deposits and it lies at the same water depths (1,900-
491 2,700 m). Although both deposits are clearly separated by the Rhone deep-sea turbiditic
492 valley (Droz and Bellaiche, 1985), it is quite likely that their emplacement is coeval,
493 share common trigger mechanisms and that may even correspond to a single event.

494 Megaturbidites are interpreted as the possible product of massive slope failures that
495 evolved into turbidity current(s) eventually deposited and trapped in the deepest part of
496 closed oceanic basins like in the Mediterranean (Cita and Aloisi, 2000; Reeder et al.,
497 2000). Exceptional high-impact hazards capable of broadly shaking or reworking

498 sediments on slopes such as volcanic eruptions, earthquakes and tsunamis have been
499 suggested as a trigger mechanism (San Pedro et al., 2017), but environment-climatic
500 driven triggers such as sea-level change or gas hydrate destabilisation are also evoked
501 (Reeder et al., 2000; Rothwell et al., 2000). A 8–10 m thick dominantly muddy
502 megaturbidite fills the whole Balearic Abyssal Plain over 60,000 km². In seismic data it
503 appears as a laterally continuous, acoustically transparent layer (Rothwell et al., 1998).
504 The source remains unknown but thickening and coarsening of the basal sand of the
505 megabed towards the north suggests emplacement from that direction (Rothwell et al.,
506 1998). The calibration of the weighted mean radiocarbon age obtained on top of the
507 megabed by Rothwell et al. (1998) gives a 2 sigma age comprised between 20.3 and 20.9
508 ka cal BP with a median probability of 20.6 ka cal BP (Reimer et al., 2013) but the group
509 of dates obtained is bracketed between 19.5 and 21.7 ka cal BP (Fig. 12). Therefore, ages
510 of both RWMTD and Balearic Abyssal Plain megaturbidite are the same within 2-sigma
511 confidence interval and no chronological order can be given between the two deposits,
512 reinforcing the possibility of a genetic link compatible with the proposed northern
513 source. However, the exceptional volume of the Balearic Abyssal Plain megaturbidite
514 shows that the related mass movement was likely efficiently evacuated from the source
515 failure, which is not the case of the RWMTD and REMTD. Therefore, even though the
516 RWMTD and REMTD may have contributed to feed the megaturbidite, the failure source
517 must be also sought in adjacent areas characterized by recurrent slope failures like the
518 Ligurian margin (Ioualalen et al., 2010; Migeon et al., 2011).

519

520 **5.5. Consequences on sediment routing in the western Gulf of Lions rise and** 521 **Rhone fan**

522 Sedimentation and sediment transfer processes in the GoL and Catalan-Ebro margins
523 are characterized by high sediment input from the Rhone and Ebro River and by
524 numerous canyons dissecting the outer shelf and slope efficiently draining sediments
525 towards the base of slope. The transfer was obviously efficient during the LGM lowstand
526 with the growth of the deep-sea fans and sedimentary ridges (Beaudouin et al., 2004;
527 Jallet and Giresse, 2005; Lombo Tombo et al., 2015; Melki et al., 2009). Even during the
528 Holocene highstand, although sediment fluxes at the shelf break are several orders of
529 magnitude lower than during the LGM, canyons remain an efficient pathway as they can
530 focus high amplitude hydro-sedimentary processes with a strong imprint on the sea bed
531 morphology (Canals et al., 2006; Lastras et al., 2007b; Palanques et al., 2006; Payo-Payo
532 et al., 2017) and even deposit sandy turbidites at the base of slope (Dennielou et al.,
533 2009). In the western part of the GoL, the Sète canyon network, the La Fonera canyon
534 and the Clots del Puget canyon presently reach the base of slope and vanish at ca. 2300
535 m (Fig. 1).

536 The longitudinal concave-up shape of the buried valley along the western flank of the
537 Rhone fan, in the direct prolongation and in good fit with the concave-up longitudinal
538 shape of the Sète canyon and the Valencia channel (Figs. 10B, C, D and 13A), shows that
539 during the LGM, prior to the emplacement of the RWMTD, the western GoL canyon
540 drainage network and the Ebro-Valence canyon drainage networks were coalescing and
541 that, probably, the Valencia fan was collecting significantly more important volumes of
542 sediment (Fig. 13A). The presence of such an important erosional channel questions
543 about the sediment source and flow capable of developing and maintaining this conduit.
544 The presence of an axial incision in several canyons (Bourcart, Herault and Marti)
545 suggests that these canyons heads were connected with major rivers during the last
546 glaciation and were fed by sustained confined turbidity currents (Baztan et al., 2005).

547 This is confirmed by the mapping of the LGM paleo-fluvial drainage network on the shelf
548 that shows that the Herault canyon was fed by the Rhone River (Jouet et al., 2006) and
549 may have supplied frequent turbiditic flows to develop the valley.

550 The burying and clogging of this channel resulted in a major reorganisation of the
551 sediment routing in the north-western Mediterranean. It is not possible to determine
552 the magnitude of the decrease in the quantity of sediment supply into the Valencia
553 channel, but this question could be easily addressed by collecting sediments cores along
554 the Valencia channel, both upstream and downstream of the channels coalescence. The
555 RWMTD was not found inside the Valencia valley, while it is still visible inside the
556 extremity of the Clots del Puget/Entrant de Palamos valley where both valleys coalesced
557 (Fig. 8D). Indeed, the RWMTD may have never been engaged inside the Valencia
558 channel, but it is also possible that deposits have been eroded and removed from the
559 valley. This is also suggested by evidences of upstream erosion in the Valencia channel,
560 in the order of several meters per thousand years since the LGM (Amblas et al., 2011).

561 A close examination of seabed morphology at the outlet of the Sète canyon network
562 shows large erosive bedforms in the distal reaches, including grooves and crescent
563 scours (Lastras et al., 2007b) and shows that the seabed has a concave-up shape on top
564 of the RWMTD (Fig. 4B and 4D). This is indicative that bed-load sediment transport with
565 dominantly bypassing and erosive processes have persisted down the Sète canyon
566 network during the LGM after the emplacement of the RWMTD and have started the
567 excavation of a new drainage at the same location of the buried one. Shallow, lobe-
568 shaped deposits, such as the Sète lobe (Droz et al., 2001), at the extremity of the canyon
569 are also suspected (Fig. 13B). There are also evidences of currently active hydro-
570 sedimentary processes in the Cap de Creus canyon such as dense water cascading

571 capable of transporting huge quantities of sediment (Canals et al., 2006; Lastras et al.,
572 2007b; Palanques et al., 2009) further suggesting that excavation is still ongoing.

573 We have shown that several sediment failures that fed the RWMTD have affected the
574 Rhone fan deposits and that headscars have even nearly reached the perched valley (Fig.
575 4B and 6A). The last, westward, avulsion of the Rhone deep-sea channel occurred
576 shortly after the emplacement of the RWMTD as indicated by the subsequently
577 deposited neofan resting on top of the RWMTD (Figs. 5 to 8) (Droz and Bellaiche, 1985;
578 Torres et al., 1997). Interestingly, the channel avulsion occurred in an area where the
579 RWMTD extends onto the Rhone levee and that can be interpreted as a failure area
580 similar to that further north (Fig. 4B and 5C). Therefore one can argue that channel
581 avulsion may have been triggered after breaching of the levee by the failure of the levee,
582 although downstream clogging of the Rhone channel is also evoked (Droz and Bellaiche,
583 1985).

584 The major disruptions in the sediment routing occurred shortly (ca. 3 ky) before the
585 onset of the post-glacial sea level rise at ca. 18.5 cal. ka BP and the sediment starvation
586 of slope and base-of-slope fans consecutive to the backstepping of sediment depocenters
587 onto the shelf (Berné et al., 2007; Lombo Tombo et al., 2015). Therefore the
588 consequences on the sedimentation in the Valencia fan, the final sink, may not be well
589 visible and recorded. It is possible to extrapolate the consequences during a future
590 lowstand. Since there are evidences that the concave-up morphology at the base of slope
591 has already started to recover, one can argue that during a future lowstand the recovery
592 may be complete and that the Valencia channel may collect again the sediments from the
593 Sète canyon network, but, in addition and this is a major contrast with the LGM, the
594 neochannel avulsion will possibly also route the Rhone sediment into the Valencia
595 channel and fan making it the collector from the two major north-western

596 Mediterranean rivers, the Ebro and the Rhone. However, this would be a temporary
597 situation because the Rhone levees display several collapses prone to trigger breaches
598 and new channel avulsions (Fig. 4B and 6A).

599

600 **5.6. Significance for sediment routing in the submarine realm**

601 Modification of sediment transport pathways in the terrestrial realm by rerouting of
602 rivers after hillslope landslides or glacier retreat is well documented and major ($>10^5$
603 m^3) terrestrial landslides can instantaneously modify river pathways for periods of
604 times relevant to landscape evolution ($>10^4$ yr) (Ouimet et al., 2007; Shugar et al., 2017).
605 Large landslides can also act as a primary control on channel morphology and
606 longitudinal river profiles, modify the adjustment of rivers to regional tectonic, climatic,
607 and lithologic forcing (Ouimet et al., 2007), and therefore influence the volume and rates
608 of sediment delivered into the oceans. Though marine landslide volumes are up to three
609 order of magnitude larger than their aerial counterparts (Hampton et al., 1996; Urgeles
610 and Camerlenghi, 2013) and are major elements of sedimentary margin development,
611 their contribution to deep-sea sediment routing is not well documented. As a
612 consequence of their widespread occurrence in turbidite systems, landslides, mass
613 transport deposits or mass transport complexes play a significant role in the topography
614 of channels or slopes, affect the resulting accommodation space, the development and
615 bifurcation of deep-sea channel, and *in fine* can control the routing and dispersal of
616 sediment at the fan scale (Armitage et al., 2009; Bernhardt et al., 2012; Corella et al.,
617 2016; Kawamura et al., 2010; Kneller et al., 2016; Ortiz-Karpf et al., 2015). However, a
618 fundamental modification of a deep-sea sediment transport network by a single
619 submarine mass transport deposit at continental margin scale seems unprecedented.
620 Noteworthy, the present case also involves rapid turbidite accumulation showing that

621 rapid changes of sediment routing may occur in areas of massive sediment deposition
622 prone to rapid evolution of submarine morphologies. We suggest that the converging
623 pattern of the canyon network as well as the semi-confined morphology at the base of
624 slope of the western part of the GoL created a receptacle suitable for rapid infill and
625 blocking of canyons.

626

627 **6. Conclusions**

628 A comprehensive mapping of the Rhone RWMTD was performed, based on seismic data
629 collected during several oceanographic campaigns between 1997 and 2008. The
630 RWMTD emplaced on the western flank of the Rhone fan and involved sediment from
631 the base of slope and from the adjacent Rhone fan levee. The RWMTD covers a surface of
632 6800 km². It represents a volume of 160 km³ of folded and contorted laminated clayey
633 high-density stiff sediments that have spread over 180 km.

634 Our results show that :

- 635 - Large mass transport deposits can be obscured in settings where sedimentation
636 rates are high. This underlines the importance of integrated (swath bathymetric,
637 seismics, core data) studies, and also suggests that hazard catalogues constructed
638 from seafloor morphology alone may be incomplete.
- 639 - Mass wasting is a major process of the margin development in the GoL and more
640 generally in the north-western Mediterranean. Several very large events occurred
641 within a very small time window in the Western Mediterranean (Rhone Western and
642 Eastern mass transport deposits and Balearic Abyssal Plain megaturbidite) and
643 account for a significant proportion of the stratigraphy. Though probably not
644 genetically linked, they occurred in period of time of large sediment transport into
645 the base of slope during the Last Glacial Maximum.

646 - Large landslide deposits can fundamentally modify sediment routing systems in the
647 marine realm at margin scale. Mass wasting must therefore be considered as a major
648 internal forcing on sediment dispersal. These drastic events can have a major impact
649 on downstream sedimentation at the base of slope and abyssal plains where
650 sedimentation is therefore not only controlled by externally forced fluctuations of
651 sea level and sediment flux.

652 It can be pointed out that the emplacement of the RWMTD in the lowstand systems tract,
653 shortly (1-2 ky) before the onset of the post-glacial sea level rise and Rhone fan
654 sediment starvation (Lombo Tombo et al., 2015), is conform to the Exxon sequence
655 stratigraphy sea-level based model.

656

657 **Acknowledgements**

658 We thank chief scientists, shipboard scientific parties, captains and crews of
659 oceanographic campaigns that allowed collection of the data used in this paper.
660 IFREMER's technical staff from sediment analysis platform (René Kerbrat, Gilbert Floch,
661 Mickael Rovere, Angélique Roubi) and from Service Cartographie, Traitement de
662 Données et Instrumentation (CTDI) is thank for its help. I.J. was supported by a post-doc
663 grant from Institut Carnot IFREMER EDROME, a program from ANR (Agence Nationale
664 de la Recherche). This work was supported by the European Training Network SLATE
665 (Submarine Landslides and their impact on European continental margins) within the
666 Framework Programme for Research and Innovation Horizon 2020 under Grant
667 Agreement No 721403. We thank Jason D. Chaytor and Mike A. Clare for their
668 substantial and constructive reviews and guest editor Veerle Huvenne for the careful
669 final reading that greatly improved the manuscript. This paper is dedicated to Jean-
670 Pierre Henriot who was the head of IFREMER's "Département Géosciences Marines"

671 between 1990 and 1995. As a Director, Jean-Pierre had a strong imprint on the
672 development of studies on sedimentary environments within the Geosciences
673 Department of IFREMER.

674

675 **Sample list**

676 Core MD01-2435: <http://igsn.org/BFBGX-88347>

677 Core KSGC-10: <http://igsn.org/BFBGX-87938>

678 Core MD01-2438: <http://igsn.org/BFBGX-88349>

679

680 **References**

681 Alonso, B. and Maldonado, A., 1990. Late Quaternary sedimentation patterns of the Ebro
682 turbidite systems (northwestern Mediterranean): Two styles of deep-sea
683 deposition. *Marine Geology*, 95(3): 353-377. [https://doi.org/10.1016/0025-](https://doi.org/10.1016/0025-3227(90)90124-3)
684 [3227\(90\)90124-3](https://doi.org/10.1016/0025-3227(90)90124-3)

685 Amblas, D., Canals, M., Urgeles, R., Lastras, G., Liqueste, C., Hughes-Clarke, J.E., Casamor,
686 J.L. and Calafat, A.M., 2006. Morphogenetic mesoscale analysis of the
687 northeastern Iberian margin, NW Mediterranean Basin. *Marine Geology*, 234(1-
688 4): 3-20. <https://doi.org/10.1016/j.margeo.2006.09.009>

689 Amblas, D., Gerber, T.P., Canals, M., Pratson, L.F., Urgeles, R., Lastras, G. and Calafat, A.M.,
690 2011. Transient erosion in the Valencia Trough turbidite systems, NW
691 Mediterranean Basin. *Geomorphology*, 130(3-4): 173-184.
692 <http://dx.doi.org/10.1016/j.geomorph.2011.03.013>

693 Armitage, D.A., Romans, B.W., Covault, J.A. and Graham, S.A., 2009. The Influence of
694 Mass-Transport-Deposit Surface Topography on the Evolution of Turbidite
695 Architecture: The Sierra Contreras, Tres Pasos Formation (Cretaceous), Southern

696 Chile. *Journal of Sédimentary Research*, 79(5): 287-301.
697 <https://doi.org/10.2110/jsr.2009.035>

698 Aslanian, D., Géli, L. and Olivet, J.-L., 2006. SARDINIA cruise, RV L'Atalante.
699 <http://dx.doi.org/10.17600/6010150>

700 Bassetti, M.A., Berné, S., Jouet, G., Taviani, M., Dennielou, B., Flores, J.-A., Gaillot, A.,
701 Gelfort, R., Lafuerza, S. and Sultan, N., 2008. 100-ka and rapid sea-level changes
702 recorded by prograding shelf sand bodies in the Gulf of Lions (Western
703 Mediterranean). *Geochemistry, Geophysics, and Geosystems*, 9(11): Q11R05.
704 <https://doi.org/doi:10.1029/2007GC001854>

705 Baztan, J., Berné, S., Olivet, J.-L., Rabineau, M., Aslanian, D., Gaudin, M., Réhault, J.-P. and
706 Canals, M., 2005. Axial incision, the key to understand submarine canyon
707 evolution (in the western gulf of Lion). *Marine and Petroleum Geology*, 22(6-7):
708 805-806. <https://doi.org/10.1016/j.marpetgeo.2005.03.011>

709 Beaudouin, C., Dennielou, B., Melki, T., Guichard, F., Kallel, N., Berne, S. and Huchon, A.,
710 2004. The Late-Quaternary climatic signal recorded in a deep-sea turbiditic levee
711 (Rhône Neofan, Gulf of Lions, NW Mediterranean): palynological constraints.
712 *Sedimentary Geology*, 172(1-2): 85-97.
713 <https://doi.org/10.1016/j.sedgeo.2004.07.008>

714 Bellaiche, G., Coutellier, V. and Droz, L., 1986. Seismic evidence of widespread mass
715 transport deposits in the Rhône deep-sea fan: Their role in the fan construction.
716 *Marine Geology*, 71(3): 327-340. [https://doi.org/10.1016/0025-](https://doi.org/10.1016/0025-3227(86)90076-9)
717 [3227\(86\)90076-9](https://doi.org/10.1016/0025-3227(86)90076-9)

718 Berné, S., 2000. MARION cruise, RV Le Suroît. <http://dx.doi.org/10.17600/20110>

719 Berné, S. and Dennielou, B., 2008. RHOSOS cruise, RV Le Suroît.
720 <http://dx.doi.org/10.17600/8020040>

721 Berné, S., Jouet, G., Bassetti, M.A., Dennielou, B. and Taviani, M., 2007. Late Glacial to
722 Preboreal sea-level rise recorded by the Rhone deltaic system (NW
723 Mediterranean). *Marine Geology*, 245(1-4): 65-88.
724 <https://doi.org/10.1016/j.margeo.2007.07.006>

725 Berné, S., Loubrieu, B. and embarquée, I.E.C., 1999. Canyons et processus sédimentaires
726 récents sur la marge occidentale du Golfe du Lion. Premiers résultats de la
727 campagne Calmar. *Comptes Rendus de l'Académie des Sciences - Series IIA -*
728 *Earth and Planetary Science*, 328(7): 471-477. [https://doi.org/10.1016/S1251-](https://doi.org/10.1016/S1251-8050(99)80148-7)
729 [8050\(99\)80148-7](https://doi.org/10.1016/S1251-8050(99)80148-7)

730 Berné, S., Satra, C., Aloïsi, J.-C., Baztan, J., Dennielou, B., Droz, L., Dos Reis, A.T., Lofi, J.,
731 Méar, Y. and Marina, R., 2004. Carte morpho-bathymétrique du Golfe du Lion,
732 notice explicative. Ifremer, QUAÉ, [http://www.quae.com/fr/r411-le-golfe-du-](http://www.quae.com/fr/r411-le-golfe-du-lion-carte-morpho-bathymetrique.html)
733 [lion-carte-morpho-bathymetrique.html](http://www.quae.com/fr/r411-le-golfe-du-lion-carte-morpho-bathymetrique.html)

734 Bernhardt, A., Stright, L. and Lowe, D.R., 2012. Channelized debris-flow deposits and
735 their impact on turbidity currents: The Puchkirchen axial channel belt in the
736 Austrian Molasse Basin. *Sedimentology*, 59(7): 2042-2070.
737 <https://doi.org/10.1111/j.1365-3091.2012.01334.x>

738 Biscara, L., Hanquiez, V., Leynaud, D., Marieu, V., Mulder, T., Gallissaires, J.M., Crespin, J.P.,
739 Braccini, E. and Garlan, T., 2012. Submarine slide initiation and evolution
740 offshore Pointe Odden, Gabon ,Â Analysis from annual bathymetric data
741 (2004,Â2009). *Marine Geology*, 299-302: 43-50.
742 <https://doi.org/10.1016/j.margeo.2011.11.008>

743 Bonnel, C., Dennielou, B., Berné, S., Mulder, T. and Droz, L., 2005. Architecture and
744 depositional pattern of the Rhône Neofan and recent gravity activity in the Gulf of

745 Lions (Western Mediterranean). *Marine and Petroleum Geology*, 22(6-7): 827-
746 843. <https://doi.org/10.1016/j.marpetgeo.2005.03.003>

747 Bourcart, J., 1960. Carte topographique du fond de la Méditerranée Occidentale.
748 *Bulletin de l'Institut Océanographique*, 1163: 1-20.

749 Bourillet, J.-F., Damy, G., Dussud, L., Sultan, N., Woerther, P. and Migeon, S., 2007.
750 Behaviour of a piston corer from accelerometers and new insights on quality of
751 the recovery, Proceedings of the 6th International Off shore Site Investigation
752 and Geotechnics Conference: Confronting New Challenges and Sharing
753 Knowledge, 11-13 September 2007, London, UK, pp. 57-62.

754 Bryn, P., Berg, K., Forsberg, C.F., Solheim, A. and Kvalstad, T.J., 2005. Explaining the
755 Storegga Slide. *Marine and Petroleum Geology*, 22(1): 11-19.
756 <https://doi.org/10.1016/j.marpetgeo.2004.12.003>

757 Bugge, T., Belderson, R. and Kenyon, N.H., 1988. The Storegga slide. *Philosophical*
758 *Transactions of the Royal Society of London. Series A, Mathematical and Physical*
759 *Sciences*, 325(1586): 357. <https://doi.org/10.1098/rsta.1988.0055>

760 Canals, M., Puig, P., Durrieu de Madron, X., Heussner, S., Palanques, A. and Fabres, J.,
761 2006. Flushing submarine canyons. *Nature*, 444(7117): 354-355.
762 <https://doi.org/10.1038/nature05271>

763 Canals, M., Serra, J. and Riba, O., 1983. Toponímia de la Mar Catalano-Balear. *Bol. Soc.*
764 *Hist. Nat Balears*, 1982(2): 48-58.
765 [http://www.raco.cat/index.php/BolletiSHNBalears/article/download/171046/
766 244849](http://www.raco.cat/index.php/BolletiSHNBalears/article/download/171046/244849)

767 Cita, M.B. and Aloisi, G., 2000. Deep-sea tsunami deposits triggered by the explosion of
768 Santorini (3500y BP), eastern Mediterranean. *Sedimentary Geology*, 135(1): 181-
769 203. [https://doi.org/10.1016/S0037-0738\(00\)00071-3](https://doi.org/10.1016/S0037-0738(00)00071-3)

770 Clare, M.A., Hughes Clarke, J.E., Talling, P.J., Cartigny, M.J.B. and Pratomo, D.G., 2016.
771 Preconditioning and triggering of offshore slope failures and turbidity currents
772 revealed by most detailed monitoring yet at a fjord-head delta. *Earth and*
773 *planetary science letters*, 450: 208-220.
774 <https://doi.org/10.1016/j.epsl.2016.06.021>

775 Clark, P.U., Archer, D., Pollard, D., Blum, J.D., Rial, J.A., Brovkin, V., Mix, A.C., Pisias, N.G.
776 and Roy, M., 2006. The middle Pleistocene transition: characteristics,
777 mechanisms, and implications for long-term changes in atmospheric pCO₂.
778 *Quaternary Science Reviews*, 25(23): 3150-3184.
779 <https://doi.org/10.1016/j.quascirev.2006.07.008>

780 Cochonat, P., 2001. GMO1 cruise, RV Le Suroît. <http://dx.doi.org/10.17600/1020040>

781 Collot, J.-Y., Lewis, K., Lamarche, G. and Lallemand, S., 2001. The giant Ruatoria debris
782 avalanche on the northern Hikurangi margin, New Zealand: Result of oblique
783 seamount subduction. *Journal of Geophysical Research: Solid Earth*, 106(B9):
784 19271-19297. <https://doi.org/10.1029/2001JB900004>

785 Corella, J.P., Loizeau, J.L., Kremer, K., Hilbe, M., Gerard, J., le Dantec, N., Stark, N.,
786 González-Quijano, M. and Girardclos, S., 2016. The role of mass-transport
787 deposits and turbidites in shaping modern lacustrine deepwater channels.
788 *Marine and Petroleum Geology*, 77: 515-525.
789 <https://doi.org/10.1016/j.marpetgeo.2016.07.004>

790 Coutellier, V., 1985. Mise en évidence et rôle des mouvements gravitaires dans
791 l'évolution de la marge continentale : exemple des marges du Golfe du Lion et de
792 la Provence Occidentale. PhD Thesis, Université Pierre et Marie Curie (Paris VI),
793 197 pp.

794 Croguennec, C., Ruffine, L., Dennielou, B., Baudin, F.o., Caprais, J.-C., Guyader, V., Bayon,
795 G., Brandily, C., Le Bruchec, J., Bollinger, C., Germain, Y., Droz, L., Babonneau, N.
796 and Rabouille, C., 2017. Evidence and age estimation of mass wasting at the distal
797 lobe of the Congo deep-sea fan. *Deep Sea Research Part II: Topical Studies in*
798 *Oceanography*, 142: 50-63. <https://doi.org/10.1016/j.dsr2.2016.12.013>

799 De Blasio, F.V. and Elverhøi, A., 2011. Properties of Mass-Transport Deposits as Inferred
800 from Dynamic Modeling of Subaqueous Mass Wasting: A Short Review. In: R.C.
801 Shipp, P. Weimer and H.W. Posamentier (Editors), *Mass-Transport Deposits in*
802 *Deepwater Settings*. SEPM Society for Sedimentary Geology.
803 <https://doi.org/10.2110/sepmsp.096.499>

804 De Blasio, F.V., Elverhøi, A., Issler, D., Harbitz, C.B., Bryn, P. and Lien, R., 2005. On the
805 dynamics of subaqueous clay rich gravity mass flows—the giant Storegga slide,
806 Norway. *Marine and Petroleum Geology*, 22(1): 179-186.
807 <https://doi.org/10.1016/j.marpetgeo.2004.10.014>

808 Dennielou, B., Droz, L., Babonneau, N., Jacq, C.l., Bonnel, C.d., Picot, M., Le Saout, M., Saout,
809 Y., Bez, M., Savoye, B., Olu, K. and Rabouille, C., 2017. Morphology, structure,
810 composition and build-up processes of the active channel-mouth lobe complex of
811 the Congo deep-sea fan with inputs from remotely operated underwater vehicle
812 (ROV) multibeam and video surveys. *Deep Sea Research Part II: Topical Studies*
813 *in Oceanography*, 142: 25-49. <https://doi.org/10.1016/j.dsr2.2017.03.010>

814 Dennielou, B., Huchon, A., Beaudouin, C. and Berné, S., 2006. Vertical grain-size
815 variability within a turbidite levee: Autocyclicity or allocyclicity? A case study
816 from the Rhone neofan, Gulf of Lions, Western Mediterranean. *Marine Geology*,
817 234(1-4): 191-213. <https://doi.org/10.1016/j.margeo.2006.09.019>

818 Dennielou, B., Jallet, L., Sultan, N., Jouet, G., Giresse, P., Voisset, M. and Berné, S., 2009.
819 Post-glacial persistence of turbiditic activity within the Rhône deep-sea turbidite
820 system (Gulf of Lions, Western Mediterranean): Linking the outer shelf and the
821 basin sedimentary records. *Marine Geology*, 257(1-4): 65-86.
822 <http://dx.doi.org/10.1016/j.margeo.2008.10.013>

823 dos Reis, A.T., Gorini, C. and Mauffret, A., 2005. Implications of salt-sediment
824 interactions on the architecture of the Gulf of Lions deep-water sedimentary
825 systems—western Mediterranean Sea. *Marine and Petroleum Geology*, 22(6):
826 713-746. <https://doi.org/10.1016/j.marpetgeo.2005.03.006>

827 Droz, L., 1983. L'éventail sous-marin profond du Rhône (Golfe du lion) : grands traits
828 morphologiques et structure semi-profonde. PhD Thesis, Université Paris VI,
829 Paris, 195 pp. <http://archimer.ifremer.fr/doc/00042/15327/>

830 Droz, L., 2003. PROGRES cruise, RV Le Suroît. <http://dx.doi.org/10.17600/3020080>

831 Droz, L. and Bellaiche, G., 1985. Rhone Deep-Sea Fan: morphostructure and growth
832 pattern. *American Association of Petroleum Geologists Bulletin*, 69: 460-479.

833 Droz, L., Kergoat, R., Cochonat, P. and Berné, S., 2001. Recent sedimentary events in the
834 western Gulf of Lions (Western Mediterranean). *Marine Geology*, 176(1-4): 23-
835 37. [https://doi.org/10.1016/S0025-3227\(01\)00147-5](https://doi.org/10.1016/S0025-3227(01)00147-5)

836 Droz, L., Reis, A.T.d., Rabineau, M., Berné, S. and Bellaiche, G., 2006. Quaternary turbidite
837 systems on the northern margins of the Balearic Basin (Western Mediterranean):
838 a synthesis. *Geo-Marine Letters*, 26(6): 347-359.
839 <https://doi.org/10.1007/s00367-006-0044-0>

840 Dugan, B., 2012. Petrophysical and consolidation behavior of mass transport deposits
841 from the northern Gulf of Mexico, IODP Expedition 308. *Marine Geology*, 315-
842 318: 98-107. <https://doi.org/10.1016/j.margeo.2012.05.001>

843 Gales, J.A., Leat, P.T., Larter, R.D., Kuhn, G., Hillenbrand, C.D., Graham, A.G.C., Mitchell,
844 N.C., Tate, A.J., Buys, G.B. and Jokat, W., 2014. Large-scale submarine landslides,
845 channel and gully systems on the southern Weddell Sea margin, Antarctica.
846 *Marine Geology*, 348: 73-87. <https://doi.org/10.1016/j.margeo.2013.12.002>

847 Garziglia, S., Migeon, S., Ducassou, E., Loncke, L. and Mascle, J., 2008. Mass-transport
848 deposits on the Rosetta province (NW Nile deep-sea turbidite system, Egyptian
849 margin): Characteristics, distribution, and potential causal processes. *Marine*
850 *Geology*, 250(3-4): 180-198. <https://doi.org/doi:10.1016/j.margeo.2008.01.016>

851 Gaullier, V., 1993. Diapirisme salifère et dynamique sédimentaire dans le bassin liguro-
852 provençal : données sismiques et modèles analogiques. Thèse d'Université
853 Thesis, Université Pierre et Marie Curie (Paris VI), 327 pp.
854 <http://archimer.ifremer.fr/doc/00034/14509/>

855 Gaullier, V., Antonini, E., Benkhelil, J. and Got, H., 1998. Recent gravity-driven
856 sedimentary bodies in the North-Balearic Basin: geometry and quantification.
857 *Comptes Rendus de l'Academie des Sciences - Series IIA - Earth and Planetary*
858 *Science*, 327(10): 677-684. [https://doi.org/10.1016/S1251-8050\(99\)80025-1](https://doi.org/10.1016/S1251-8050(99)80025-1)

859 Haflidason, H., Lien, R., Sejrup, H.P., Forsberg, C.F. and Bryn, P., 2005. The dating and
860 morphometry of the Storegga Slide. *Marine and Petroleum Geology*, 22(1): 123-
861 136. <https://doi.org/10.1016/j.marpetgeo.2004.10.008>

862 Hampton, M.A., Lee, H.J. and Locat, J., 1996. Submarine landslides. *Reviews of*
863 *Geophysics*, 34(1): 33-59. <https://doi.org/10.1029/95RG03287>

864 Hsü, K.J., Cita, M.B. and Ryan, W.B.F., 1973. The origin of the Mediterranean evaporites.
865 In: W.B.F. Ryan and K.J. Hsü (Editors), Leg 13, Init. Rep. Deep Sea Drill. Proj., pp.
866 1203-1231. <https://doi.org/doi:10.2973/dsdp.proc.13.1973>

867 Huppertz, T.J., Piper, D.J.W., Mosher, D.C. and Jenner, K., 2010. The Significance of Mass-
868 Transport Deposits for the Evolution of a Proglacial Continental Slope. In: D.C.
869 Mosher et al. (Editors), Submarine Mass Movements and Their Consequences.
870 Springer Netherlands, Dordrecht, pp. 631-641. [https://doi.org/10.1007/978-90-](https://doi.org/10.1007/978-90-481-3071-9_51)
871 [481-3071-9_51](https://doi.org/10.1007/978-90-481-3071-9_51)

872 IFREMER/CIESM, 2011. Morpho-bathymetry of the Mediterranean Sea. QUAЕ,
873 [http://www.quae.com/en/r770-morpho-bathymetry-of-the-mediterranean-](http://www.quae.com/en/r770-morpho-bathymetry-of-the-mediterranean-sea.html)
874 [sea.html](http://www.quae.com/en/r770-morpho-bathymetry-of-the-mediterranean-sea.html)

875 Imbo, Y., De Batist, M., Canals, M., Prieto, M.J. and Baraza, J., 2003. The Gebra Slide: a
876 submarine slide on the Trinity Peninsula Margin, Antarctica. *Marine Geology*,
877 193(3): 235-252. [https://doi.org/10.1016/S0025-3227\(02\)00664-3](https://doi.org/10.1016/S0025-3227(02)00664-3)

878 Ioualalen, M., Migeon, S. and Sardoux, O., 2010. Landslide tsunami vulnerability in the
879 Ligurian Sea: case study of the 1979 October 16 Nice international airport
880 submarine landslide and of identified geological mass failures. *Geophysical*
881 *Journal International*, 181(2): 724-740. [https://doi.org/10.1111/j.1365-](https://doi.org/10.1111/j.1365-246X.2010.04572.x)
882 [246X.2010.04572.x](https://doi.org/10.1111/j.1365-246X.2010.04572.x)

883 Issler, D., De Blasio, F.V., Elverhøj, A., Bryn, P. and Lien, R., 2005. Scaling behaviour of
884 clay-rich submarine debris flows. *Marine and Petroleum Geology*, 22(1): 187-
885 194. <https://doi.org/10.1016/j.marpetgeo.2004.10.015>

886 Jallet, L. and Giresse, P., 2005. Construction of the Pyreneo-Languedocian Sedimentary
887 Ridge and associated sediment waves in the deep western Gulf of Lions (Western
888 Mediterranean). *Marine and Petroleum Geology*, 22(6-7): 865-888.
889 <https://doi.org/10.1016/j.marpetgeo.2005.03.008>

890 Jansen, E., Befring, S., Bugge, T., Eidvin, T., Holtedahl, H. and Sejrup, H.P., 1987. Large
891 submarine slides on the Norwegian continental margin: Sediments, transport and

892 timing. *Marine Geology*, 78(1): 77-107. <https://doi.org/10.1016/0025->
893 3227(87)90069-7

894 Jégou, I., 2008. Etude de la transition chenal-levées/lobes dans les systèmes
895 turbiditiques récents : Application à l'éventail turbiditique de l'Amazone et au
896 Néofan du Petit-Rhône. Doctorat Thesis, Université de Brest, Brest, 350 pp.
897 <http://archimer.ifremer.fr/doc/00000/6796/>

898 Joanne, C., Collot, J.-Y., Lamarche, G. and Migeon, S.b., 2010. Continental slope
899 reconstruction after a giant mass failure, the example of the Matakaoa Margin,
900 New Zealand. *Marine Geology*, 268(1): 67-84.
901 <https://doi.org/10.1016/j.margeo.2009.10.013>

902 Jouet, G., Berne, S., Rabineau, M., Bassetti, M.A., Bernier, P., Dennielou, B., Sierro, F.J.,
903 Flores, J.A. and Taviani, M., 2006. Shoreface migrations at the shelf edge and sea-
904 level changes around the Last Glacial Maximum (Gulf of Lions, NW
905 Mediterranean). *Marine Geology*, 234(1-4): 21-42.
906 <https://doi.org/10.1016/j.margeo.2006.09.012>

907 Kawamura, K., Kanamatsu, T., Kinoshita, M., Saito, S., Shibata, T., Fujino, K., Misawa, A.
908 and Burmeister, K.C., 2010. Redistribution of Sediments by Submarine Landslides
909 on the Eastern Nankai Accretionary Prism. In: D.C. Mosher et al. (Editors),
910 Submarine Mass Movements and Their Consequences. Springer Netherlands,
911 Dordrecht, pp. 313-322. https://doi.org/10.1007/978-90-481-3071-9_26

912 Kelner, M., Migeon, S., Tric, E., Couboulex, F., Dano, A. and Lebourg, T., 2014. Recent
913 Morphological Changes of the Nice Continental Slope. In: G. Lollino, A. Manconi, J.
914 Locat, Y. Huang and M. Canals Artigas (Editors), *Engineering Geology for Society
915 and Territory*. Springer, Cham, 4, pp. 221-225. <https://doi.org/10.1007/978-3->
916 319-08660-6_42

917 Kneller, B., Dykstra, M., Fairweather, L. and Milana, J.P., 2016. Mass-transport and slope
918 accommodation: Implications for turbidite sandstone reservoirs. AAPG Bulletin,
919 100(2): 213-235.

920 Lastras, G., Canals, M., Amblas, D., Frigola, J., Urgeles, R., Calafat, A.M. and Acosta, J.,
921 2007a. Slope instability along the northeastern Iberian and Balearic continental
922 margins. *Geologica Acta: an international earth science journal*, 5(1): 35-48.
923 <http://www.redalyc.org/articulo.oa?id=50550103>

924 Lastras, G., Canals, M., Hughes-Clarke, J.E., Moreno, A., De Batist, M., Masson, D.G. and P.,
925 C., 2002. Seafloor imagery from the BIG'95 debris flow, western Mediterranean.
926 *Geology*, 30(10): 871-874. [https://doi.org/10.1130/0091-](https://doi.org/10.1130/0091-7613(2002)030%3C0871:SIFTBD%3E2.0.CO;2)
927 [7613\(2002\)030%3C0871:SIFTBD%3E2.0.CO;2](https://doi.org/10.1130/0091-7613(2002)030%3C0871:SIFTBD%3E2.0.CO;2)

928 Lastras, G., Canals, M., Urgeles, R., Amblas, D., Ivanov, M., Droz, L., Dennielou, B., Fabres,
929 J., Schoolmeester, T., Akhmetzhanov, A., Orange, D. and Garcia-Garcia, A., 2007b. A
930 walk down the Cap de Creus canyon, Northwestern Mediterranean Sea: Recent
931 processes inferred from morphology and sediment bedforms. *Marine Geology*,
932 246(2-4): 176-192. <https://doi.org/10.1016/j.margeo.2007.09.002>

933 Lastras, G., Canals, M., Urgeles, R., De Batist, M., Calafat, A.M. and Casamor, J.L., 2004.
934 Characterisation of the recent BIG'95 debris flow deposit on the Ebro margin,
935 Western Mediterranean Sea, after a variety of seismic reflection data. *Marine*
936 *Geology*, 213(1): 235-255. <https://doi.org/10.1016/j.margeo.2004.10.008>

937 Le Cann, C., 1987. Le diapirisme dans le bassin Liguro-provençal (Méditerranée
938 occidentale). Relations avec la tectonique et la sédimentation. Implications
939 géodynamiques. Université de Bretagne Occidentale, Brest, 296 pp.
940 <http://archimer.ifremer.fr/doc/00034/14519/>

941 Lee, H.J., 2009. Timing of occurrence of large submarine landslides on the Atlantic Ocean
942 margin. *Marine Geology*, 264(1-2): 53-64.
943 <https://doi.org/10.1016/j.margeo.2008.09.009>

944 Leroux, E., Rabineau, M., Aslanian, D., Gorini, C., Molliex, S., Bache, F., Robin, C., Droz, L.,
945 Moulin, M., Poort, J., Rubino, J.-L. and Suc, J.-P., 2017. High-resolution evolution of
946 terrigenous sediment yields in the Provence Basin during the last 6 Ma: relation
947 with climate and tectonics. *Basin research*, 29(3): 305-339.
948 <https://doi.org/10.1111/bre.12178>

949 Leroux, E., Rabineau, M., Aslanian, D., Granjeon, D., Droz, L. and Gorini, C., 2014.
950 Stratigraphic simulations of the shelf of the Gulf of Lions: testing subsidence rates
951 and sea-level curves during the Pliocene and Quaternary. *Terra Nova*, 26(3):
952 230-238. <https://doi.org/10.1111/ter.12091>

953 Lofi, J., Rabineau, M., Gorini, C., Berne, S., Clauzon, G., De Clarens, P., Dos Reis, A.T.,
954 Mountain, G.S., Ryan, W.B.F., Steckler, M.S. and Fouchet, C., 2003. Plio-Quaternary
955 prograding clinoform wedges of the western Gulf of Lion continental margin (NW
956 Mediterranean) after the Messinian Salinity Crisis. *Marine Geology*, 198(3-4):
957 289-317. [https://doi.org/10.1016/s0025-3227\(03\)00120-8](https://doi.org/10.1016/s0025-3227(03)00120-8)

958 Lombo Tombo, S., Dennielou, B., Berné, S., Bassetti, M.A., Toucanne, S., Jorry, S.J., Jouet, G.
959 and Fontanier, C., 2015. Sea-level control on turbidite activity in the Rhone
960 canyon and the upper fan during the Last Glacial Maximum and Early deglacial.
961 *Sedimentary Geology*, 323(0): 148-166.
962 <http://dx.doi.org/10.1016/j.sedgeo.2015.04.009>

963 Loubrieu, B., 1997. CALMAR97 cruise, RV L'Atalante.
964 <http://dx.doi.org/10.17600/97010120>

965 Maldonado, A., Palanques, A., Alonso, B., Kastens, K.A., Nelson, C.H., O'Connell, S. and
966 Ryan, W.B.F., 1985. Physiography and deposition on a distal deep-sea system:
967 The Valencia Fan (Northwestern Mediterranean). *Geo-marine letters*, 5(3): 157-
968 164. <https://doi.org/10.1007/bf02281633>

969 Manchuel, K., Traversa, P., Baumont, D., Cara, M., Nayman, E. and Durouchoux, C., 2017.
970 The French seismic CATalogue (FCAT-17). *Bulletin of Earthquake Engineering*.
971 <http://dx.doi.org/10.1007/s10518-017-0236-1>

972 Mauffrey, M.A., Berné, S., Jouet, G., Giresse, P. and Gaudin, M., 2015. Sea-level control on
973 the connection between shelf-edge deltas and the Bourcart canyon head (western
974 Mediterranean) during the last glacial/interglacial cycle. *Marine Geology*, 370: 1-
975 19. <http://dx.doi.org/10.1016/j.margeo.2015.09.010>

976 Mazières, A., Gillet, H., Castelle, B., Mulder, T., Guyot, C., Garlan, T. and Mallet, C., 2014.
977 High-resolution morphobathymetric analysis and evolution of Capbreton
978 submarine canyon head (Southeast Bay of Biscay—French Atlantic Coast) over
979 the last decade using descriptive and numerical modeling. *Marine Geology*, 351:
980 1-12. <https://doi.org/10.1016/j.margeo.2014.03.001>

981 McHugh, C.M.G., Damuth, J.E., Gartner, S., Katz, M.E. and Mountain, G.S., 1996. Oligocene
982 to Holocene mass-transport deposits of the New Jersey continental margin and
983 their correlation to sequence boundaries. In: G.S. Mountain, K.G. Miller, P. Blum,
984 C.W. Poag and D.C. Twichell (Editors), *Proceedings of the Ocean Drilling Program,*
985 *Scientific Results*, 150, pp. 189-228.
986 <http://dx.doi.org/10.2973/odp.proc.sr.150.016.1996>

987 Méar, Y. and Gensous, B., 1993. Processus d'édification d'une unite interlobe; application
988 au deep-sea fan du Petit-Rhône. *Comptes Rendus de l'Académie des Sciences*,

989 Serie II, Mécanique, Physique, Chimie, Sciences de l'Univers, Sciences de la Terre,
990 317(12): 1633-1640.

991 Melki, T., Kallel, N., Jorissen, F.J., Guichard, F., Dennielou, B., Berné, S., Labeyrie, L. and
992 Fontugne, M., 2009. Abrupt climate change, sea surface salinity and
993 paleoproductivity in the western Mediterranean Sea (Gulf of Lion) during the last
994 28 kyr. *Palaeogeography, Palaeoclimatology, Palaeoecology*, 279(1-2): 96-113.
995 <https://doi.org/10.1016/j.palaeo.2009.05.005>

996 Micallef, A., Mountjoy, J.J., Canals, M. and Lastras, G., 2012. Deep-Seated Bedrock
997 Landslides and Submarine Canyon Evolution in an Active Tectonic Margin: Cook
998 Strait, New Zealand. In: Y. Yamada et al. (Editors), *Submarine Mass Movements
999 and Their Consequences*. Springer Netherlands, Dordrecht, pp. 201-212.
1000 https://doi.org/10.1007/978-94-007-2162-3_18

1001 Migeon, S., Cattaneo, A., Hassoun, V., Larroque, C., Corradi, N., Fanucci, F., Dano, A., de
1002 Lepinay, B.M., Sage, F. and Gorini, C., 2011. Morphology, distribution and origin of
1003 recent submarine landslides of the Ligurian Margin (North-western
1004 Mediterranean): some insights into geohazard assessment. *Marine Geophysical
1005 Research*, 32(1-2): 225-243. <https://doi.org/10.1007/s11001-011-9123-3>

1006 Mohrig, D., Ellis, C., Parker, G., Whipple, K.X. and Hondzo, M., 1998. Hydroplaning of
1007 subaqueous debris flows. *GSA Bulletin*, 110(3): 387-394.
1008 [https://doi.org/10.1130/0016-7606\(1998\)110<0387:HOSDF>2.3.CO;2](https://doi.org/10.1130/0016-7606(1998)110<0387:HOSDF>2.3.CO;2)

1009 Mulder, T., 2011. Chapter 2 - Gravity Processes and Deposits on Continental Slope, Rise
1010 and Abyssal Plains. In: H. HüNeke and T. Mulder (Editors), *Developments in
1011 Sedimentology*. Elsevier, 63, pp. 25-148. [https://doi.org/10.1016/B978-0-444-
1012 53000-4.00002-0](https://doi.org/10.1016/B978-0-444-53000-4.00002-0)

1013 Mulder, T. and Cochonat, P., 1996. Classification of offshore mass movements, *Journal of*
1014 *Sedimentary Research*, pp. 43-57.

1015 Nelson, C.H., Escutia, C., Damuth, J.E. and Twichell, J.D.C., 2011. Interplay of Mass-
1016 Transport and Turbidite-System Deposits in Different Active Tectonic and
1017 Passive Continental Margin Settings: External and Local Controlling Factors. In:
1018 R.C. Shipp, P. Weimer and H.W. Posamentier (Editors), *Mass-Transport Deposits*
1019 *in Deepwater Settings*. SEPM Society for Sedimentary Geology, pp. 39-66.
1020 <https://doi.org/10.2110/sepmsp.096.039>

1021 O'Connell, S., Normark, W.R., Ryan, W.B.F. and Kenyon, N.H., 1991. An entrenched
1022 thalweg channel on the Rhône fan : interpretation from a SEABEAM and
1023 SEAMARC I survey, *SEPM Special Publication*, 46, pp. 259-270.
1024 <https://doi.org/10.2110/pec.91.09.0259>

1025 Obelcz, J., Xu, K., Georgiou, I.Y., Maloney, J., Bentley, S.J. and Miner, M.D., 2017. Sub-
1026 decadal submarine landslides are important drivers of deltaic sediment flux:
1027 Insights from the Mississippi River Delta Front. *Geology*, 45(8): 703-706.
1028 <https://doi.org/10.1130/G38688.1>

1029 Ortiz-Karpf, A., Hodgson, D.M. and McCaffrey, W.D., 2015. The role of mass-transport
1030 complexes in controlling channel avulsion and the subsequent sediment
1031 dispersal patterns on an active margin: The Magdalena Fan, offshore Colombia.
1032 *Marine and Petroleum Geology*, 64: 58-75.
1033 <https://doi.org/10.1016/j.marpetgeo.2015.01.005>

1034 Ouimet, W.B., Whipple, K.X., Royden, L.H., Sun, Z. and Chen, Z., 2007. The influence of
1035 large landslides on river incision in a transient landscape: Eastern margin of the
1036 Tibetan Plateau (Sichuan, China). *GSA Bulletin*, 119(11-12): 1462-1476.
1037 <https://doi.org/10.1130/B26136.1>

1038 Palanques, A., Durrieu de Madron, X., Puig, P., Fabres, J., Guillen, J., Calafat, A., Canals, M.,
1039 Heussner, S. and Bonnin, J., 2006. Suspended sediment fluxes and transport
1040 processes in the Gulf of Lions submarine canyons. The role of storms and dense
1041 water cascading. *Marine Geology*, 234(1-4): 43-61.
1042 <https://doi.org/10.1016/j.margeo.2006.09.002>

1043 Palanques, A., Puig, P., Latasa, M. and Scharek, R., 2009. Deep sediment transport
1044 induced by storms and dense shelf-water cascading in the northwestern
1045 Mediterranean basin. *Deep Sea Research Part I: Oceanographic Research Papers*,
1046 56(3): 425-434. <https://doi.org/10.1016/j.dsr.2008.11.002>

1047 Payo-Payo, M., Jacinto, R.S., Lastras, G., Rabineau, M., Puig, P., Martín, J., Canals, M. and
1048 Sultan, N., 2017. Numerical modeling of bottom trawling-induced sediment
1049 transport and accumulation in La Fonera submarine canyon, northwestern
1050 Mediterranean Sea. *Marine Geology*, 386: 107-125.
1051 <https://doi.org/10.1016/j.margeo.2017.02.015>

1052 Piper, D., Pirmez, C., Manley, L.P., Long, D., Flood, R.D., Normark, W. and Showers, W.,
1053 1997. Mass-transport deposits of the Amazon Fan. In: R.D. Flood, D. Piper, A.
1054 Klaus and L.C. Peterson (Editors), *Proceedings of the Ocean Drilling Program,*
1055 *Scientific Results*, 155, College Station TX, pp. 109-146.
1056 <http://dx.doi.org/doi:10.2973/odp.proc.sr.155.212.1997>

1057 Piper, D.J.W., Mosher, D.C., Gauley, B.J., Jenner, K. and Campbell, D.C., 2003. The
1058 Chronology and Recurrence of Submarine Mass Movements on the Continental
1059 Slope Off Southeastern Canada. In: J. Locat, J. Mienert and L. Boisvert (Editors),
1060 *Submarine Mass Movements and Their Consequences: 1st International*
1061 *Symposium.* Springer Netherlands, Dordrecht, pp. 299-306.
1062 https://doi.org/10.1007/978-94-010-0093-2_33

1063 Pont, D., Simonnet, J.-P. and Walter, A.V., 2002. Medium-term Changes in Suspended
1064 Sediment Delivery to the Ocean: Consequences of Catchment Heterogeneity and
1065 River Management (Rhône River, France). *Estuarine, Coastal and Shelf Science*,
1066 54(1): 1-18. <https://doi.org/10.1006/ecss.2001.0829>

1067 Popescu, I., Lericolais, G., Panin, N., Wong, H.K. and Droz, L., 2001. Late Quaternary
1068 channel avulsions on the Danube deep-sea fan, Black Sea. *Marine Geology*, 179(1-
1069 2): 25-37. [https://doi.org/10.1016/S0025-3227\(01\)00197-9](https://doi.org/10.1016/S0025-3227(01)00197-9)

1070 Rabineau, M. and Aslanian, D., 2007. SEEPGOL cruise, RV Le Suroît.
1071 <http://dx.doi.org/10.17600/7020080>

1072 Rabineau, M., Berne, S., Aslanian, D., Olivet, J.-L., Joseph, P., Guillocheau, F., Bourillet, J.-F.,
1073 Ledrezen, E. and Granjeon, D., 2005. Sedimentary sequences in the Gulf of Lion: A
1074 record of 100,000 years climatic cycles. *Marine and Petroleum Geology*, 22(6-7):
1075 775-804. <https://doi.org/10.1016/j.marpetgeo.2005.03.010>

1076 Rabineau, M., Berne, S., Ledrezen, E., Lericolais, G., Marsset, T. and Rotunno, M., 1998. 3D
1077 architecture of lowstand and transgressive Quaternary sand bodies on the outer
1078 shelf of the Gulf of Lion, France. *Marine and Petroleum Geology*, 15(5): 439-452.

1079 Rabineau, M., Berne, S., Olivet, J.-L., Aslanian, D., Guillocheau, F. and Joseph, P., 2006.
1080 Paleo sea levels reconsidered from direct observation of paleoshoreline position
1081 during Glacial Maxima (for the last 500,000 yr). *Earth and Planetary Science*
1082 *Letters*, 252(1-2): 119-137. <https://doi.org/10.1016/j.epsl.2006.09.033>

1083 Rabineau, M., Leroux, E., Aslanian, D., Bache, F., Gorini, C., Moulin, M., Molliex, S., Droz, L.,
1084 dos Reis, A.T., Rubino, J.L., Guillocheau, F. and Olivet, J.L., 2014. Quantifying
1085 subsidence and isostatic readjustment using sedimentary paleomarkers, example
1086 from the Gulf of Lion. *Earth and planetary science letters*, 388: 353-366.
1087 <https://doi.org/10.1016/j.epsl.2013.11.059>

1088 Reeder, M.S., Rothwell, R.G. and Stow, D.A.V., 2000. Influence of sea level and basin
1089 physiography on emplacement of the late Pleistocene Herodotus Basin
1090 Megaturbidite, SE Mediterranean Sea. *Marine and Petroleum Geology*, 17(2):
1091 199-218. [https://doi.org/10.1016/S0264-8172\(99\)00048-3](https://doi.org/10.1016/S0264-8172(99)00048-3)

1092 Reimer, P.J., Bard, E., Bayliss, A., Beck, J.W., Blackwell, P.G., Ramsey, C.B., Buck, C.E.,
1093 Cheng, H., Edwards, R.L., Friedrich, M., Grootes, P.M., Guilderson, T.P., Haflidason,
1094 H., Hajdas, I., Hatte, C., Heaton, T.J., Hoffmann, D.L., Hogg, A.G., Hughen, K.A.,
1095 Kaiser, K.F., Kromer, B., Manning, S.W., Niu, M., Reimer, R.W., Richards, D.A., Scott,
1096 E.M., Southon, J.R., Staff, R.A., Turney, C.S.M. and van der Plicht, J., 2013. Intcal13
1097 and Marine13 radiocarbon age calibration curves 0-50,000 Years Cal BP.
1098 *Radiocarbon*, 55(4): 1869-1887. https://doi.org/10.2458/azu_js_rc.55.16947

1099 Rothwell, R.G., Reeder, M.S., Anastasakis, G., Stow, D.A.V., Thomson, J. and Kähler, G.,
1100 2000. Low sea-level stand emplacement of megaturbidites in the western and
1101 eastern Mediterranean Sea. *Sedimentary Geology*, 135(1-4): 75-88.
1102 [https://doi.org/10.1016/S0037-0738\(00\)00064-6](https://doi.org/10.1016/S0037-0738(00)00064-6)

1103 Rothwell, R.G., Thomson, J. and Kähler, G., 1998. Low-sea-level emplacement of a very
1104 large Late Pleistocene 'megaturbidite' in the western Mediterranean Sea. *Nature*,
1105 392(6674): 377-380. <https://doi.org/10.1038/32871>

1106 San Pedro, L., Babonneau, N., Gutscher, M.A. and Cattaneo, A., 2017. Origin and
1107 chronology of the Augias deposit in the Ionian Sea (Central Mediterranean Sea),
1108 based on new regional sedimentological data. *Marine Geology*, 384: 199-213.
1109 <https://doi.org/10.1016/j.margeo.2016.05.005>

1110 Shanmugam, G. and Wang, Y., 2015. The landslide problem. *Journal of Palaeogeography*,
1111 4(2): 109-166. <http://dx.doi.org/10.3724/SP.J.1261.2015.00071>

1112 Shipp, R.C., Weimer, P. and Posamentier, H.W., 2011. Mass-Transport Deposits in
1113 Deepwater Settings: An Introduction. In: R.C. Shipp, P. Weimer and H.W.
1114 Posamentier (Editors), Mass-Transport Deposits in Deepwater Settings. SEPM
1115 Society for Sedimentary Geology. <https://doi.org/10.2110/sepmsp.096.003>

1116 Shugar, D.H., Clague, J.J., Best, J.L., Schoof, C., Willis, M.J., Copland, L. and Roe, G.H., 2017.
1117 River piracy and drainage basin reorganization led by climate-driven glacier
1118 retreat. *Nature Geoscience*, 10: 370. <https://doi.org/10.1038/ngeo2932>

1119 Sierro, F.J., Andersen, N., Bassetti, M.A., BernÈ, S., Canals, M., Curtis, J.H., Dennielou, B.,
1120 Flores, J.A., Frigola, J., Gonzalez-Mora, B., Grimalt, J.O., Hodell, D.A., Jouet, G.,
1121 PÈrez-Folgado, M. and Schneider, R., 2009. Phase relationship between sea level
1122 and abrupt climate change. *Quaternary Science Reviews*, 28(25-26): 2867-2881.
1123 <https://doi.org/10.1016/j.quascirev.2009.07.019>

1124 Skinner, L.C. and McCave, I.N., 2003. Analysis and modelling of gravity- and piston coring
1125 based on soil mechanics. *Marine Geology*, 199(1-2): 181-204.
1126 [https://doi.org/10.1016/S0025-3227\(03\)00127-0](https://doi.org/10.1016/S0025-3227(03)00127-0)

1127 Smith, D.P., Kvitek, R., Iampietro, P.J. and Wong, K., 2007. Twenty-nine months of
1128 geomorphic change in upper Monterey Canyon (2002,Äì2005). *Marine Geology*,
1129 236(1): 79-94. <https://doi.org/10.1016/j.margeo.2006.09.024>

1130 Stabholz, M., Durrieu de Madron, X., Canals, M., Khripounoff, A., Taupier-Letage, I.,
1131 Testor, P., Heussner, S., Kerhervé, P., Delsaut, N., Houpert, L., Lastras, G. and
1132 Dennielou, B., 2013. Impact of open-ocean convection on particle fluxes and
1133 sediment dynamics in the deep margin of the Gulf of Lions. *Biogeosciences*, 10(2):
1134 1097-1116. <https://doi.org/10.5194/bg-10-1097-2013>

1135 Stuiver, M., Reimer, P.J. and Reimer, R.W., 2018. CALIB 7.1 [WWW program].
1136 <http://calib.org>.

1137 Sultan, N., Gaudin, M., Berne, S., Canals, M., Urgeles, R. and Lafuerza, S., 2007. Analysis of
1138 slope failures in submarine canyon heads: An example from the Gulf of Lions.
1139 Journal of Geophysical Research, 112(F01009).
1140 <http://dx.doi.org/doi:10.1029/2005JF000408>

1141 Sultan, N. and Voisset, M., 2002. GMO2 - CARNAC cruise, RV Le Suroît.
1142 <http://dx.doi.org/10.17600/2020080>

1143 Tesson, M. and Gensous, B., 1998. L'enregistrement des cycles climatiques et eustatiques
1144 quaternaires de marges récentes du bassin Nord-Méditerranéen ; Quaternary
1145 record of climatic and eustatic cycles on modern margins of the north-
1146 mediterranean basin. Comptes Rendus de l'Académie des Sciences - Series IIA -
1147 Earth and Planetary Science, 326(2): 121-127. [https://doi.org/10.1016/S1251-](https://doi.org/10.1016/S1251-8050(97)87456-3)
1148 [8050\(97\)87456-3](https://doi.org/10.1016/S1251-8050(97)87456-3)

1149 Torres, J., Droz, L., Savoye, B., Terentieva, E., Cochonat, P., Kenyon, N.H. and Canals, M.,
1150 1997. Deep-sea avulsion and morphosedimentary evolution of the Rhône Fan
1151 Valley and Neofan during the Late Quaternary (north-western Mediterranean
1152 Sea). Sedimentology, 44: 457-477. [https://doi.org/10.1046/j.1365-](https://doi.org/10.1046/j.1365-3091.1997.d01-36.x)
1153 [3091.1997.d01-36.x](https://doi.org/10.1046/j.1365-3091.1997.d01-36.x)

1154 Torres, J., Savoye, B. and Cochonat, P., 1995. The effects of late quaternary sea-level
1155 changes on the Rhône slope sedimentation (northwestern mediterranean), as
1156 indicated by seismic stratigraphy. Journal of Sedimentary Research, B65(3): 368-
1157 387. <https://doi.org/10.1306/D4268257-2B26-11D7-8648000102C1865D>

1158 Tripsanas, E.K., Piper, D.J.W., Jenner, K.A. and Bryant, W.R., 2008. Submarine mass-
1159 transport facies: new perspectives on flow processes from cores on the eastern
1160 North American margin. Sedimentology, 55: 97-136. doi:10.1111/j.1365-
1161 3091.2007.00894.x

- 1162 Turon, J.-L., 2001. MD 123 / GEOSCIENCES 1 cruise, RV Marion Dufresne.
1163 <http://dx.doi.org/10.17600/1200050>
- 1164 Twichell, D.C., Kenyon, N.H., Parson, L.M. and McGregor, B.A., 1991. Depositional
1165 Patterns of the Mississippi Fan Surface: Evidence from GLORIA II and High-
1166 Resolution Seismic Profiles. In: P. Weimer and M.H. Link (Editors), Seismic Facies
1167 and Sedimentary Processes of Submarine Fans and Turbidite Systems. Springer
1168 New York, New York, NY, pp. 349-363. [http://dx.doi.org/10.1007/978-1-4684-
1169 8276-8_19](http://dx.doi.org/10.1007/978-1-4684-8276-8_19)
- 1170 Urgeles, R. and Camerlenghi, A., 2013. Submarine landslides of the Mediterranean Sea:
1171 Trigger mechanisms, dynamics, and frequency-magnitude distribution. Journal of
1172 Geophysical Research: Earth Surface, 118(4): 2600-2618.
1173 <http://dx.doi.org/10.1002/2013jf002720>
- 1174 Weimer, P., 1989. Sequence stratigraphy of the Mississippi fan (Plio-Pleistocene), Gulf of
1175 Mexico. Geo-marine letters, 9(4): 185-272. <https://doi.org/10.1007/bf02431072>

1177 **Figure captions**

1178 *Figure 1*

1179 Bathymetric map of the Gulf of Lions and Catalan margins with indication of main
1180 morpho-sedimentary features (white dashed lines: sedimentary deposits; black dashed
1181 lines: Mass Transport Deposits; violet dashed lines: main canyons; black solid line:
1182 current Petit-Rhone canyon/channel). Gulf of Lions canyons (Berné et al., 2004): CC: Cap
1183 de Creus, LD: Lacaze Duthier, P: Pruvost, Bc: Bourcart, He: Herault, S: Sète, CL: Catherine
1184 Laurence, M: Marti (whose coalescence forms the Sète canyons network), PR: Petit-
1185 Rhone, GR: Grand-Rhone, Ms: Marseille, PL: Planier, C: Cassidaigne. Catalan margin
1186 canyons (Canals et al., 1983): LF: La Fonera, CdP: Clots del Puget, B: Blanes. REMTD:

1187 Eastern Mass Transport Deposit, RWMTD: Western Mass Transport Deposit. Limits of
1188 sedimentary bodies are from Droz et al. (2006) except Valencia Fan from Maldonado et
1189 al. (1985).

1190

1191 *Figure 2*

1192 Location map of slides headwalls, of buried and active listric faults (dos Reis et al.,
1193 2005), of seismic lines shown in Figs 5 to 9 and of sediment cores (white dots). PLSR:
1194 Pyreneo-Languedocian Sedimentary Ridge, PRDSF: Petit-Rhone Deep-Sea Fan, PRN: Petit-
1195 Rhone Neofan, REMTD: Eastern Mass Transport Deposit, RWMTD: Western Mass
1196 Transport Deposit. See Fig. 1 for canyon names.

1197

1198 *Figure 3*

1199 Location map of used seismic data and sediment cores

1200

1201 *Figure 4*

1202 A: Seabed morphology of the study area (map of slope) with location seismic lines and
1203 sediment cores. B: zoom in on the seabed morphology on the proximal area of the
1204 Western Mass Transport Deposit (RWMTD) at the base of slope. See scars headwall
1205 superimposed on active listric faults. Thick red arrows indicate possible main sources
1206 and pathways of the RWMTD across the western levee of the Rhone fan. C: zoom in on
1207 the seabed morphology of the eastern distal area of the RWMTD showing a bulge against
1208 the Rhone fan. D: Bathymetric section A-A' and B-B' show the morphologic expression of
1209 the compression bulge. C: bathymetric sections across the Sète valley (A-A'), showing
1210 the compression bulge at the contact between the RWMTD and the Rhone fan (B-B' and
1211 C-C'). See Figs. 2 and 4A for location. PLSR: Pyreneo-Languedocian Sedimentary Ridge.

1212

1213 *Figure 5*

1214 The Rhone Western Mass Transport Deposit (RWMTD) as seen by several types of
1215 seismic: (A and C) single channel mini GI air-gun, (B) 24-channel mini-GI air-gun, (D) 6-
1216 channel 50 Hz GI air-gun, in the proximal area at the base of slope; strike lines (A, B, C),
1217 dip lines (D). Lines A and B were acquired simultaneously but with two different
1218 streamers. See the nearly transparent facies of the RWMTD on the single channel air-gun
1219 line (A) while on the 24-channel air-gun line (B) it shows internal reflections. See Figs. 2
1220 and 4A for lines location. The top (red line) and base (blue line) of the RWMTD in D are
1221 issued from the interpretation of sub-bottom profiles. PLSR: Pyreneo-Languedocian
1222 Sedimentary Ridge.

1223

1224 *Figure 6*

1225 Sub-Bottom Profiler lines (A) across the Rhone fan valley and proximal area of the
1226 Rhone Western Mass Transport Deposit (RWMTD) showing sliding of the turbiditic
1227 levee, and (B) along the central and distal area of the RWMTD. See also location and
1228 penetration of sediment cores on the RWMTD. See Figs. 2 and 4A for lines location.

1229

1230 *Figure 7*

1231 Sub-Bottom Profiler (A) and air gun (B) seismic line across the central area of the Rhone
1232 Western Mass Transport Deposit (RWMTD). See overlapping more recent deposits and
1233 erosional features (Rhone neofan deposits and channels, scours field and deposits from
1234 La Fonera canyon). The top (red line) and base (blue line) of the RWMTD are indicated.
1235 See Fig. 2 and 4A for lines location.

1236

1237 *Figure 8*

1238 Sub-Bottom Profiler line across the distal area of the Rhone Western Mass Transport
1239 Deposit (RWMTD). See infill of substratum relief (A), overlap of RWMTD on the Rhone
1240 fan (B), infill of Palamos valley (C) and confluence of Clots del Puget/Entrant de Palamós
1241 and Valencia valleys. The top (red line) and base (blue line) of the RWMTD are indicated.
1242 See Figs. 2 and 4A for lines location.

1243

1244 *Figure 9*

1245 Sub-Bottom Profiler line across the eastern side of the Rhone Western Mass Transport
1246 Deposit (RWMTD) showing overlapping and a compression bulge against the Rhone fan.
1247 The top (red line) and base (blue line) of the RWMTD are indicated. See Figs. 2 and 4A
1248 for lines location.

1249

1250 *Figure 10*

1251 Set of maps obtained after interpretation of seismic lines. A: isochron map converted
1252 into meters below seafloor of the top of the Rhone Western Mass Transport Deposit
1253 (RWMTD). White lines outline deposits that overlap the RWMTD, thick lines: Pyreneo-
1254 Langudocian Sedimentary Ridge (PLSR) and neofan, thin lines the Sète and La Fonera
1255 lobes (Droz et al., 2001). B: isochron map converted into meters below seafloor of the
1256 base of the RWMTD. White arrows outline the presently buried valleys in the
1257 prolongation of the Sète canyon. Blue dotted line (A-A') shows the location of depth
1258 profiles shown on D. C: isochore map of the RWMTD. D: Depth profiles along the buried
1259 valley in the prolongation of the Sète canyon; red: base of the RWMTD; blue: top of the
1260 RWMTD; black: present bathymetry. Listric faults (LF) offsets are visible on the
1261 bathymetry profile at the base of slope, in the RWMTD proximal area.

1262

1263 *Figure 11*

1264 Lithofacies of sediment cores collected in the Rhone Western Mass Transport Deposit
1265 (RWMTD) at proximal (core MD01-2435), central (core KSGC-10) and distal (core
1266 MD01-2438) locations. See Figs 2, 3 and 4A for location of sediment cores.

1267

1268 *Figure 12*

1269 Graphic presentation of radiocarbon dating at the base of the hemipelagic drape on top
1270 of the Rhone Western Mass Transport Deposit (RWMTD) (this paper) and of the Balearic
1271 Abyssal Plain Megabed (Rothwell et al., 1998).

1272

1273 *Figure 13*

1274 Reconstruction maps of canyons and turbidic channels drainage network and sediment
1275 routing during the Last Glacial Maximum (LGM), before (A) and after (B) the
1276 emplacement of the Rhone Western Mass Transport Deposit (RWMTD). Solid black line
1277 indicated location of the buried valley as mapped from seismic lines. Dashed black lines
1278 indicate possible location of another parallel valley and areas where the lack of seismic
1279 lines do not allow mapping the buried valley. See Fig. 1 for canyon names.

1280

1281 **Table captions**

1282 *Table 1*

1283 Oceanographic campaigns and data used in this study. See location in Fig. 3

1284

1285 *Table 2*

1286 Location and characteristics of sediment cores used in this study. See Figs. 2 and 3 for
1287 location.

1288

1289 *Table 3*

1290 Radiocarbon dating carried out on sediment cores. Calendar ages BP (Before Present)
1291 calculated with Calib 7.1 and Marine13 calibration curve (Reimer et al., 2013). $\Delta R = 48$ y
1292 ; SD = 101 y was determined after reservoir ages in the Gulf of Lions obtained from Calib
1293 7.1 marine reservoir database.

1294

1295 Table 1

Campaign	Year	Ship	Data	Reference
Calmar97	1997	R/V L'Atalante	EM12, HR 6-channel 50 Hz GI, VHR 3.5 kHz SBP	(Loubrieu, 1997)
Marion	2000	R/V Le Suroît	EM300, HR single channel and 24 channels 130 Hz mini-GI	(Berné, 2000)
Gmo1	2001	R/V Le Suroît	EM300	(Cochonat, 2001)
MD123 / Geoscience1	2001	R/V Marion Dufresne	Calypso cores	(Turon, 2001)
Gmo2-Carnac	2002	R/V Le Suroît	EM300	(Sultan and Voisset, 2002)
Progres	2003	R/V Le Suroît	EM300, HR 6-channel 50 Hz GI, VHR 2-5.2 kHz SBP	(Droz, 2003)
Sardinia	2006	R/V L'Atalante	EM12, VHR 3.5 kHz SBP	(Aslanian et al., 2006)
Melrose Seepgol	2007	R/V Le Suroît	EM300	(Rabineau and Aslanian, 2007)
Rhosos	2008	R/V Le Suroît	EM300, VHR 2-5.2 kHz SBP	(Berné and Dennielou, 2008)

1296

1297

1298 Table 2

Core	Area	Latitude	Longitude	Water depth (m)	Length (m)	IGSN
MD01-2435	Proximal area	42°15.66' N	004°47.18' E	2025	19.23	BFBGX-88347
KSGC-10	Central area	41° 55.277'N	004 44.608' E	2399	2.03	BFBGX-87938
MD01-2438	Distal area	41°14.91' N	004°29.97' E	2628	9.00	BFBGX-88349

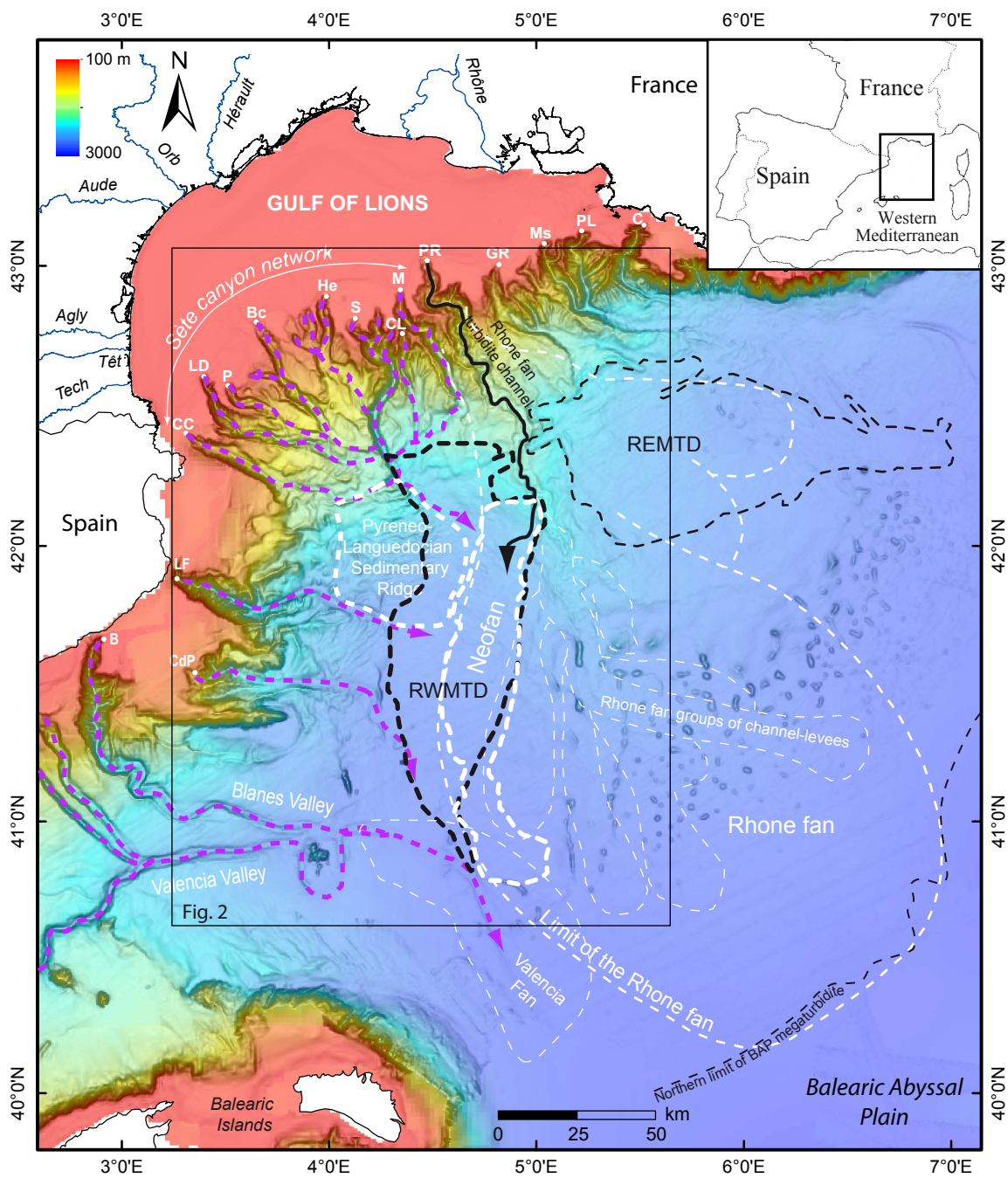
1299

1300

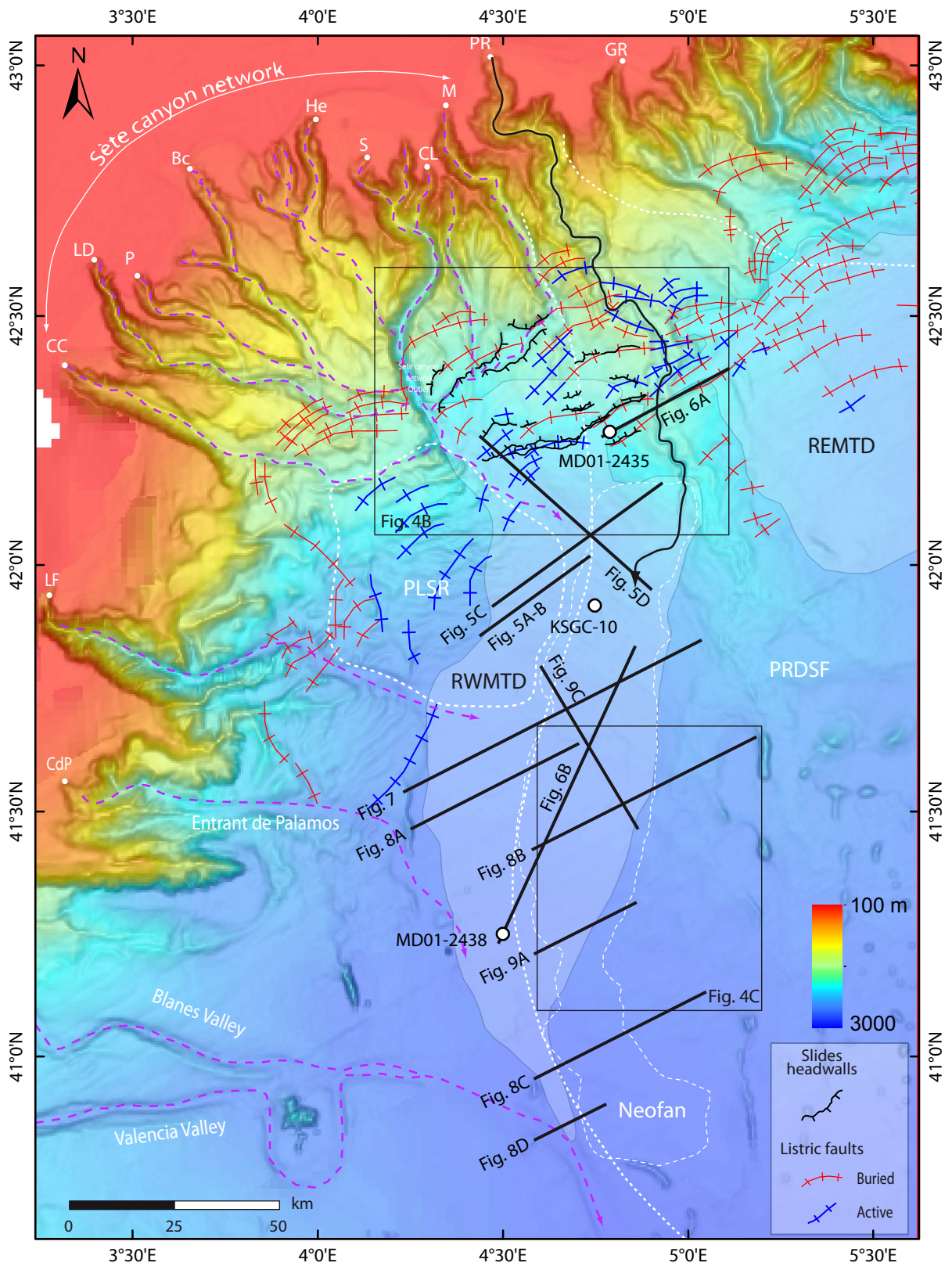
1301 Table 3

Core	Depth (cm)	Radiocarbon age (y BP)	1 σ calendar age (y BP)	2 σ calendar age (y BP)	Median calendar age (y BP)	Dated material	Lab. number
MD01-2435	22-24	12,940 \pm 70	14,379-14,980	14,163-15,134	14,666	<i>G. bulloides</i>	Poz-14639
MD01-2435	853-858	17,940 \pm 90	20,921-21,331	20,726-21,535	21,128	<i>G. bulloides</i>	Poz-14641
MD01-2435	917-923	18,310 \pm 90	21,450-21,825	21,194-21,981	21,625	<i>G. bulloides</i>	Poz-14642
MD01-2438	96-100	17,260 \pm 80	20,110-20,446	19,949-20,600	20,276	<i>G. bulloides</i>	Poz-14649
KSGC-10	1-2	840 \pm 30	318-499	239-621	415	<i>G. bulloides</i>	Poz-13817

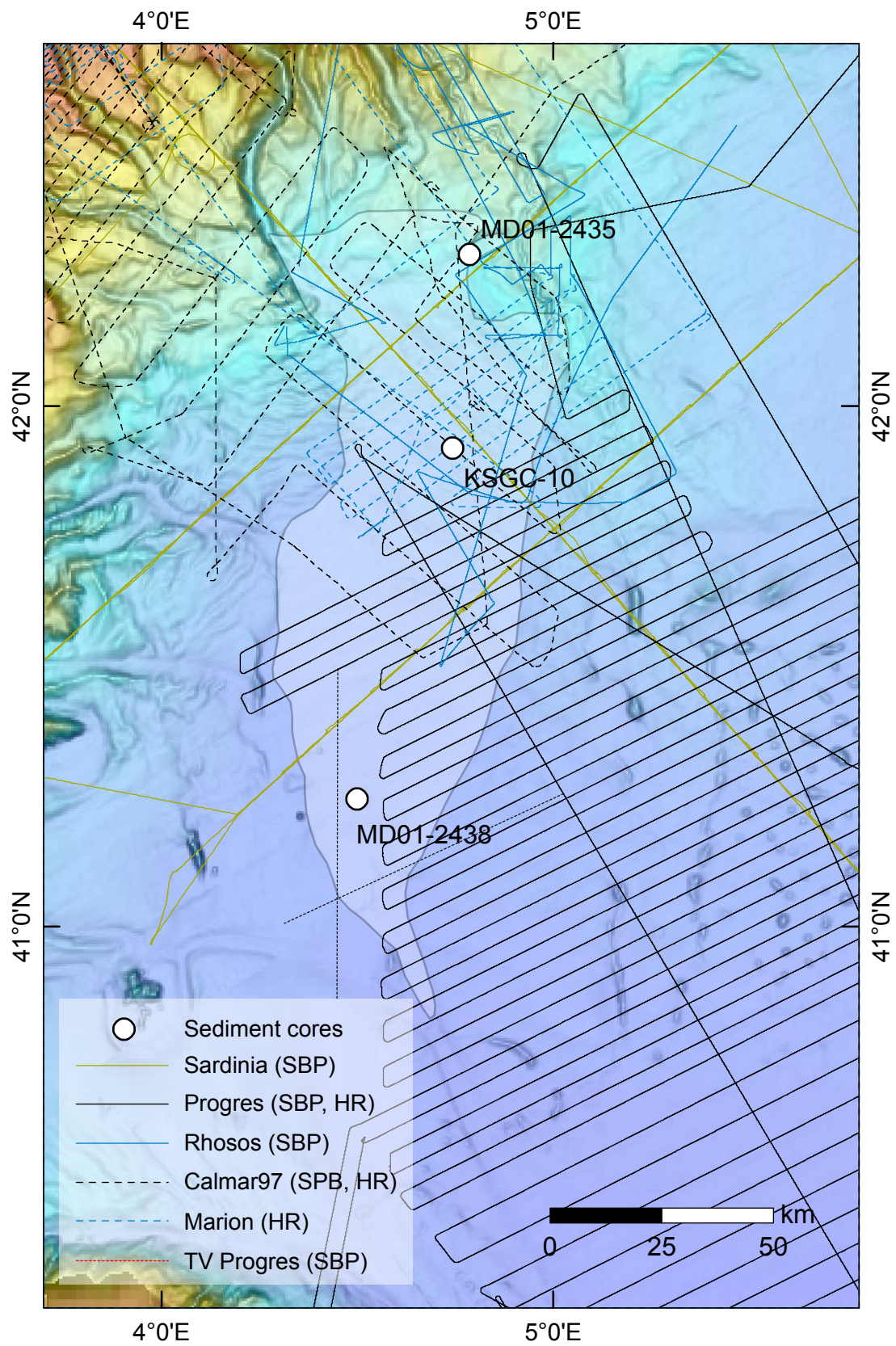
1302



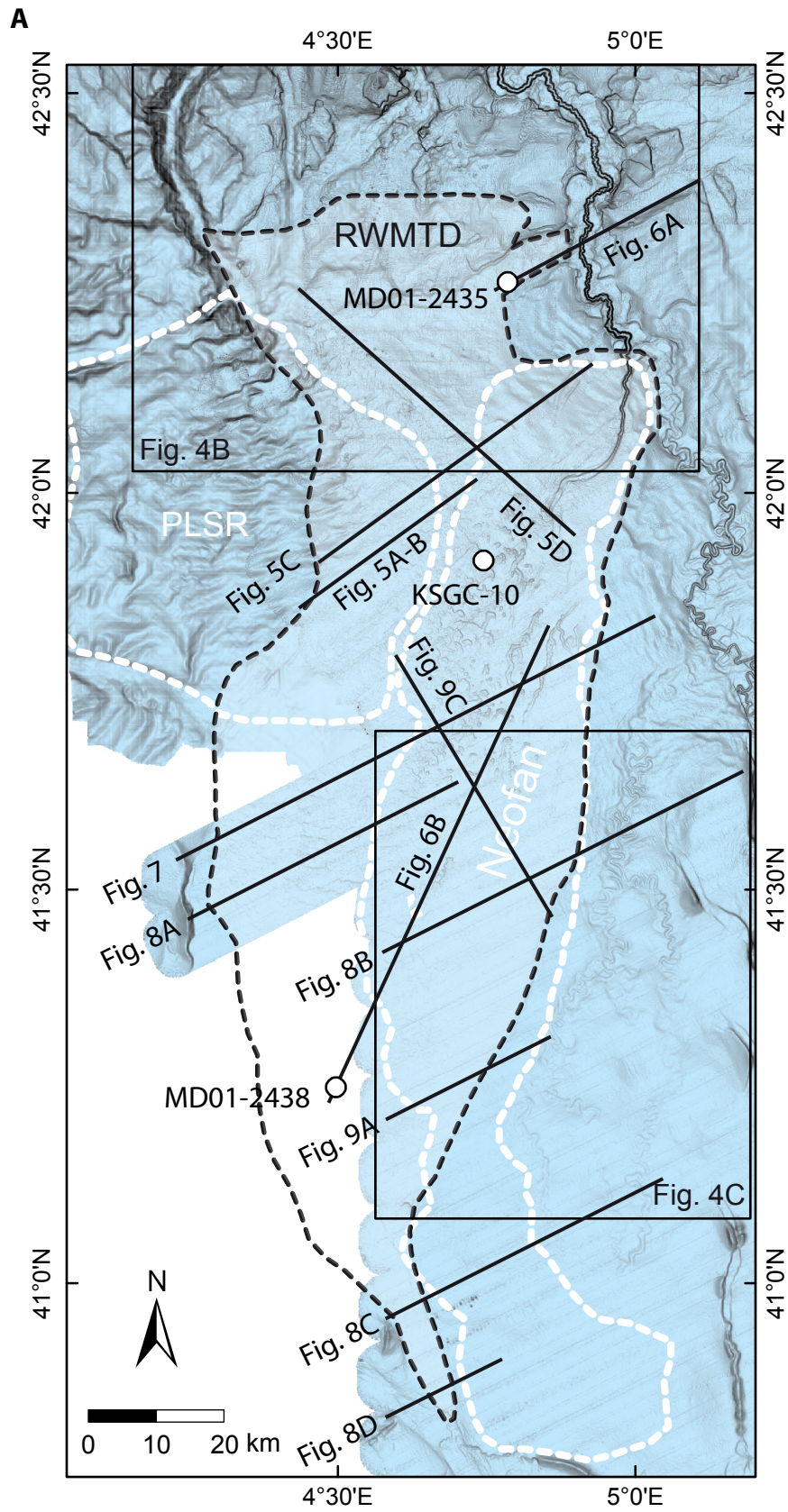
Denniellou et al. RWMTD - Figure 1



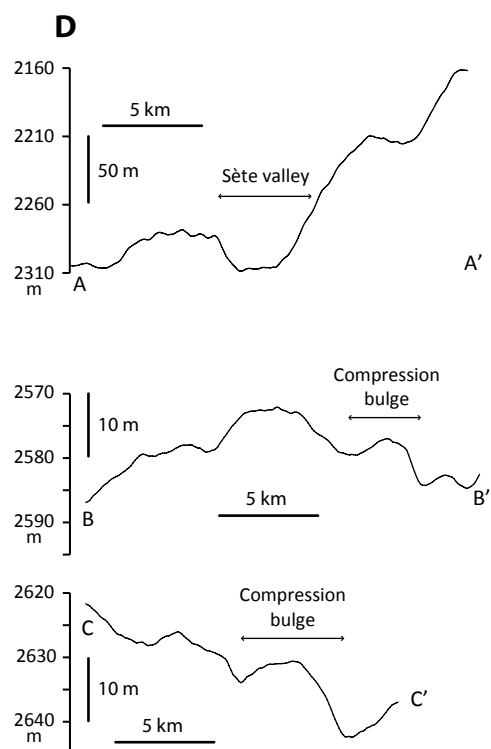
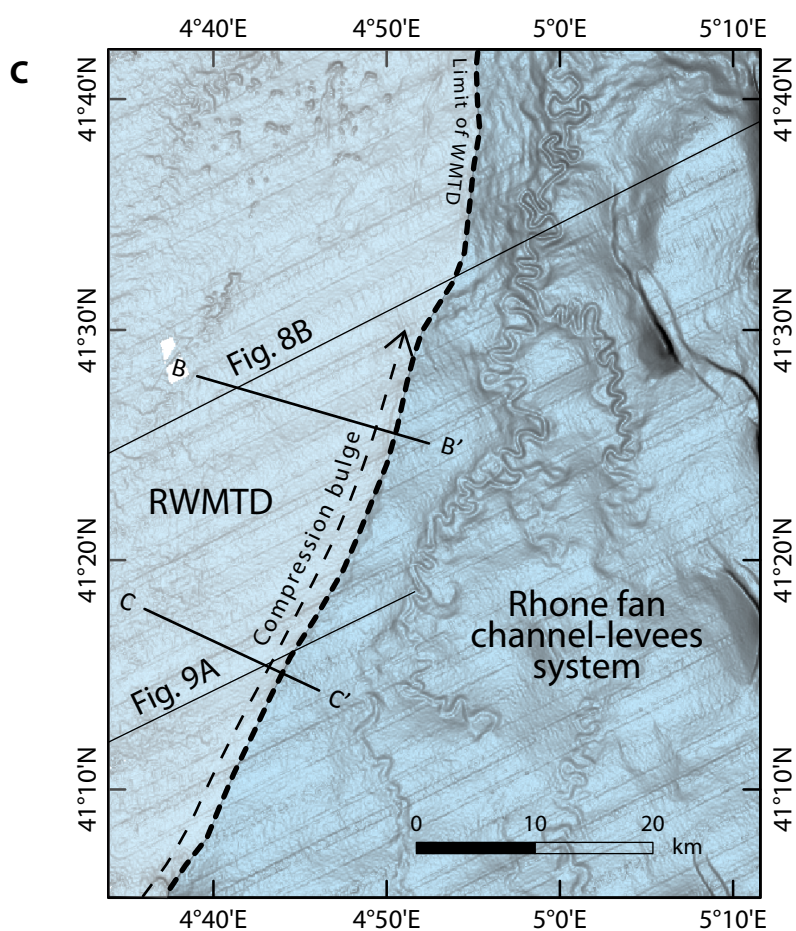
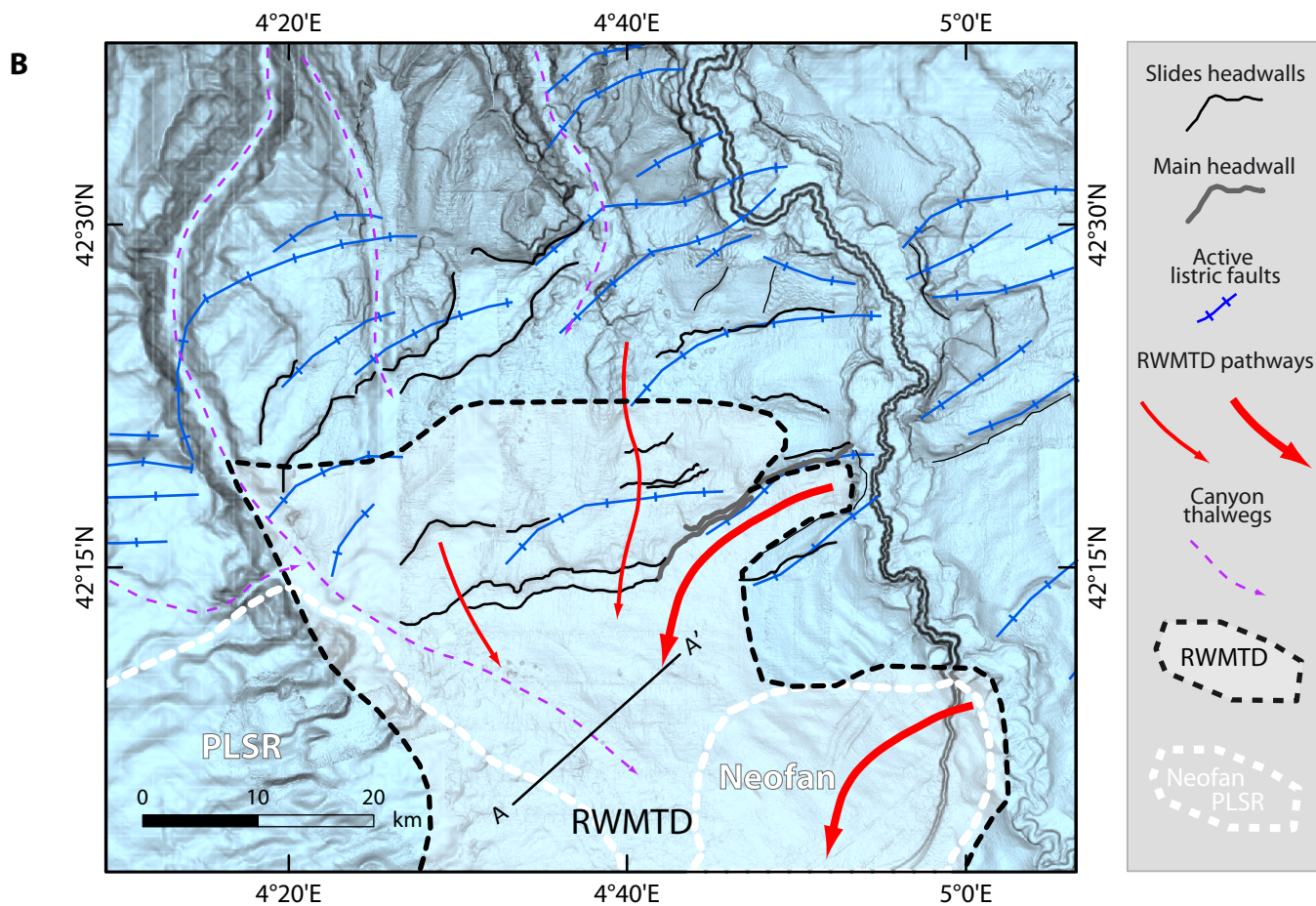
Dennielou et al. RWMTD - Figure 2



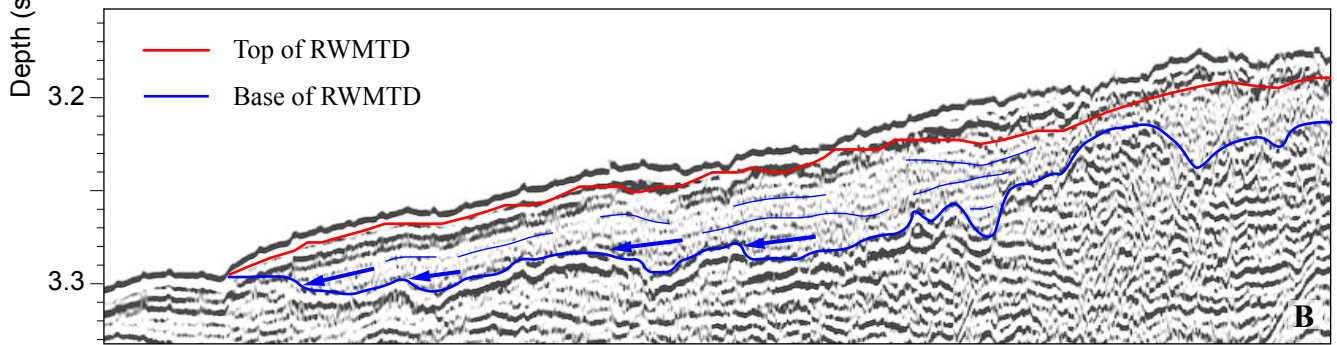
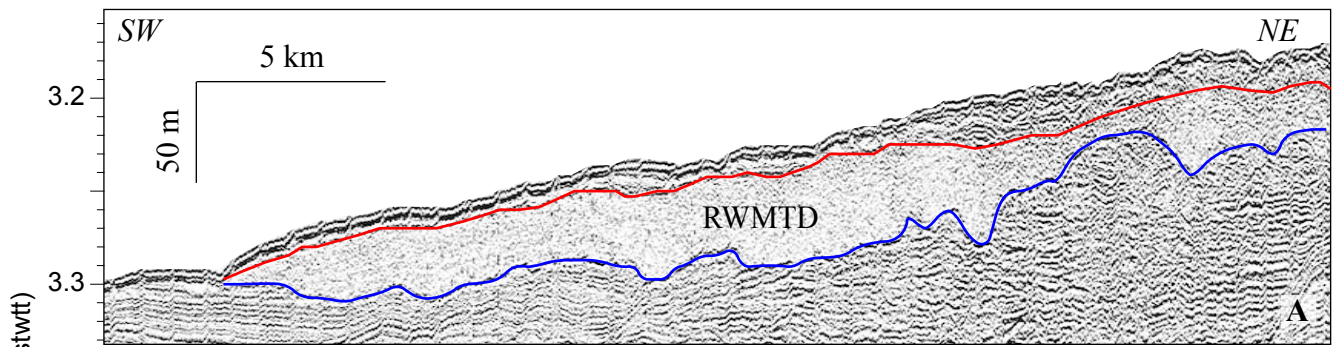
Dennielou et al. RWMTD - Figure 3



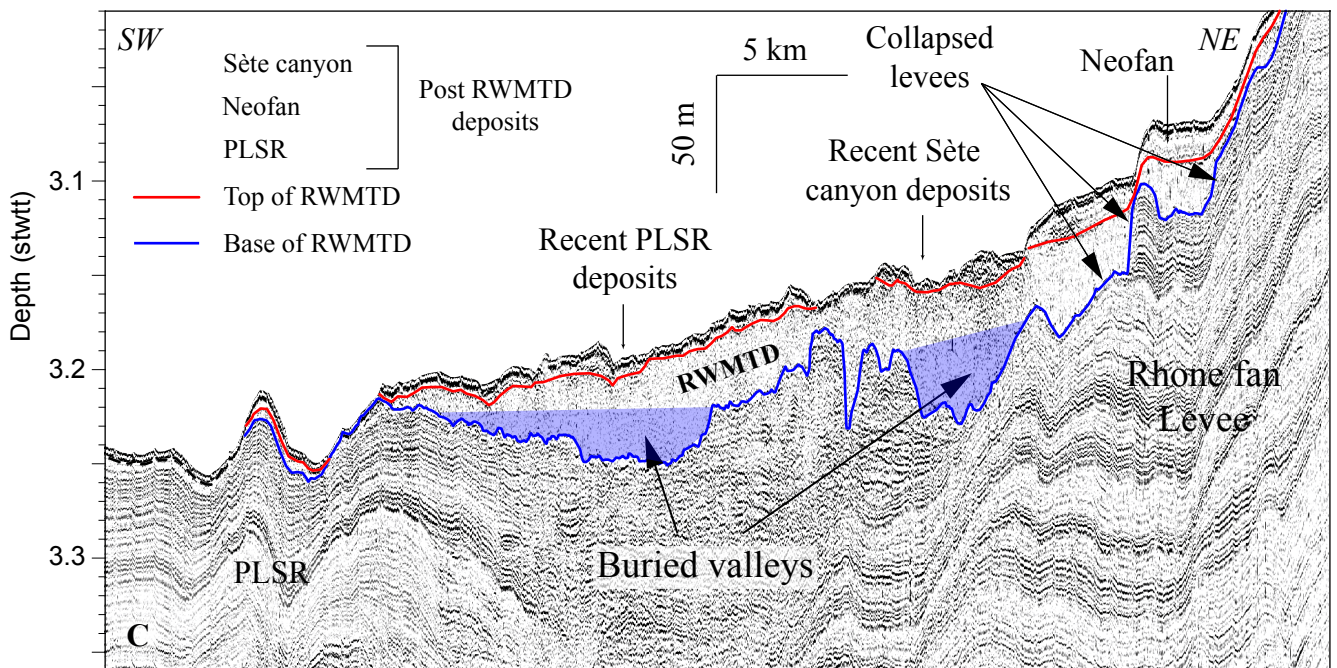
Denniellou et al. RWMTD - Figure 4



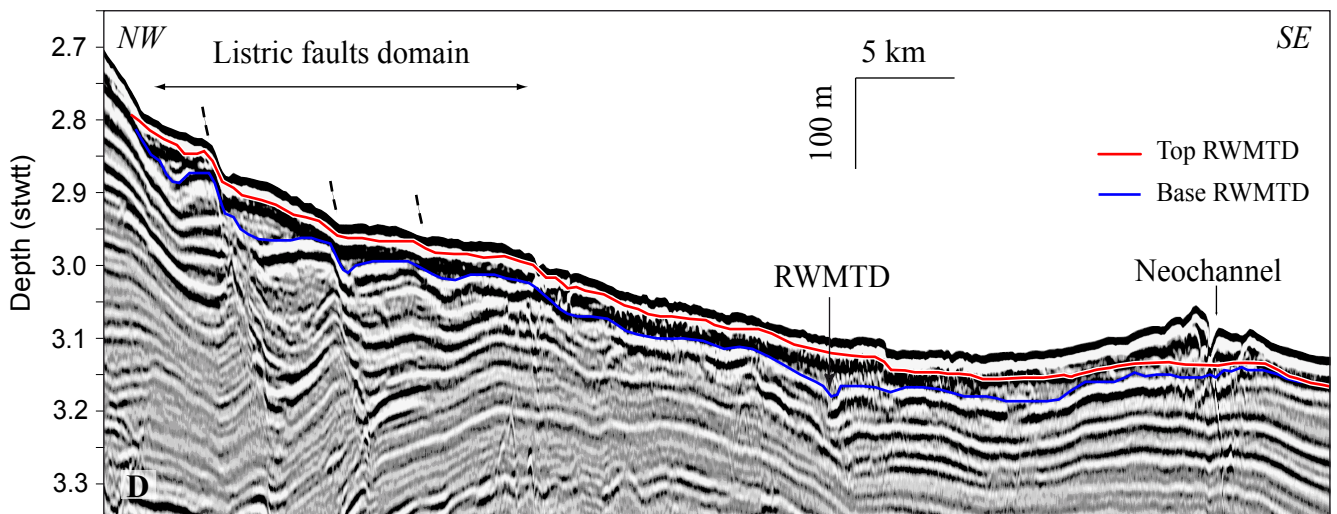
Denniellou et al. RWMTD - Figures 4A, 4B, 4C



Marion-88

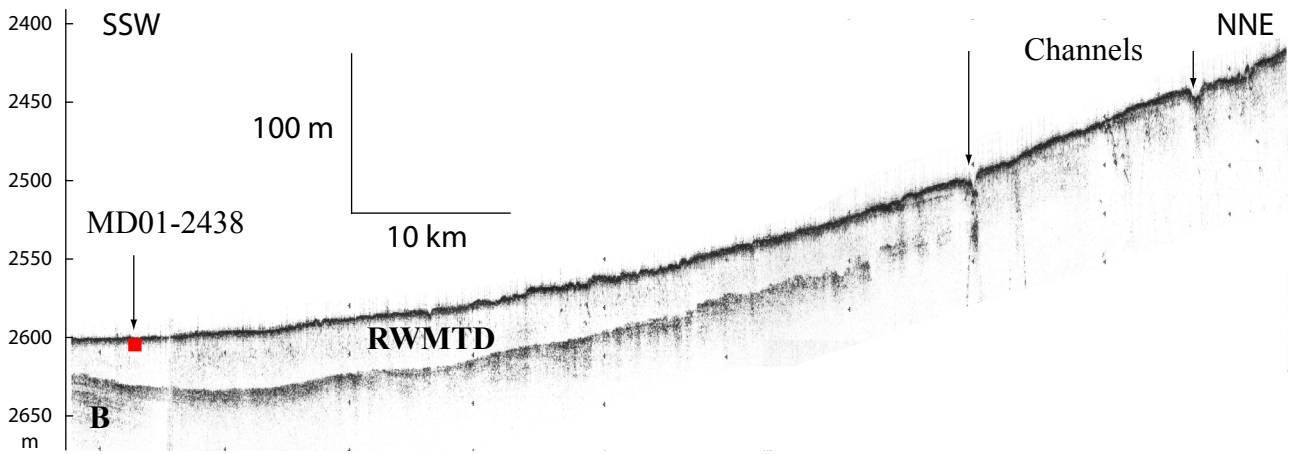
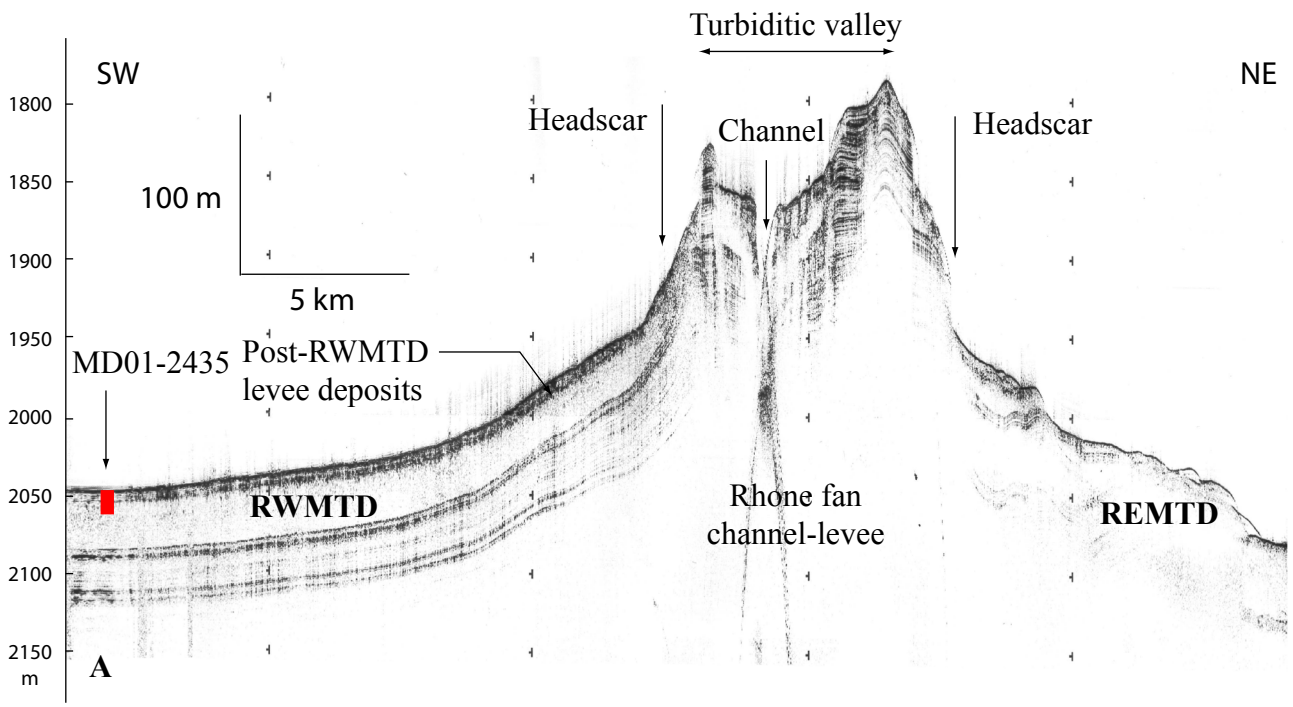


Marion-87

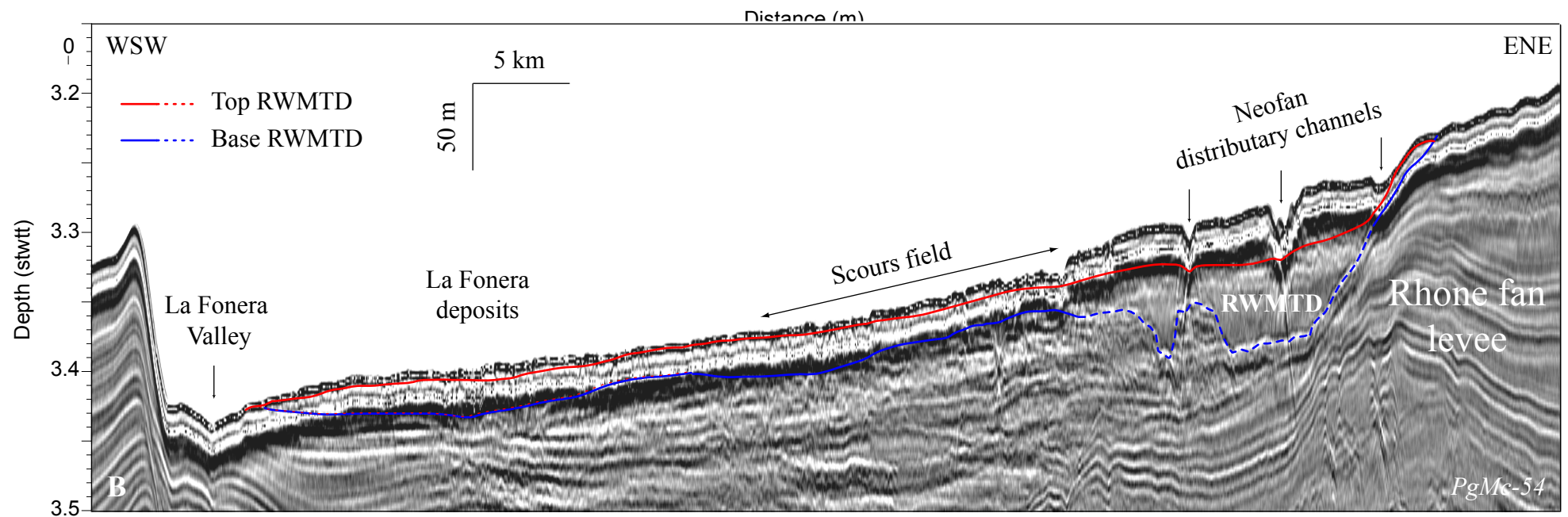
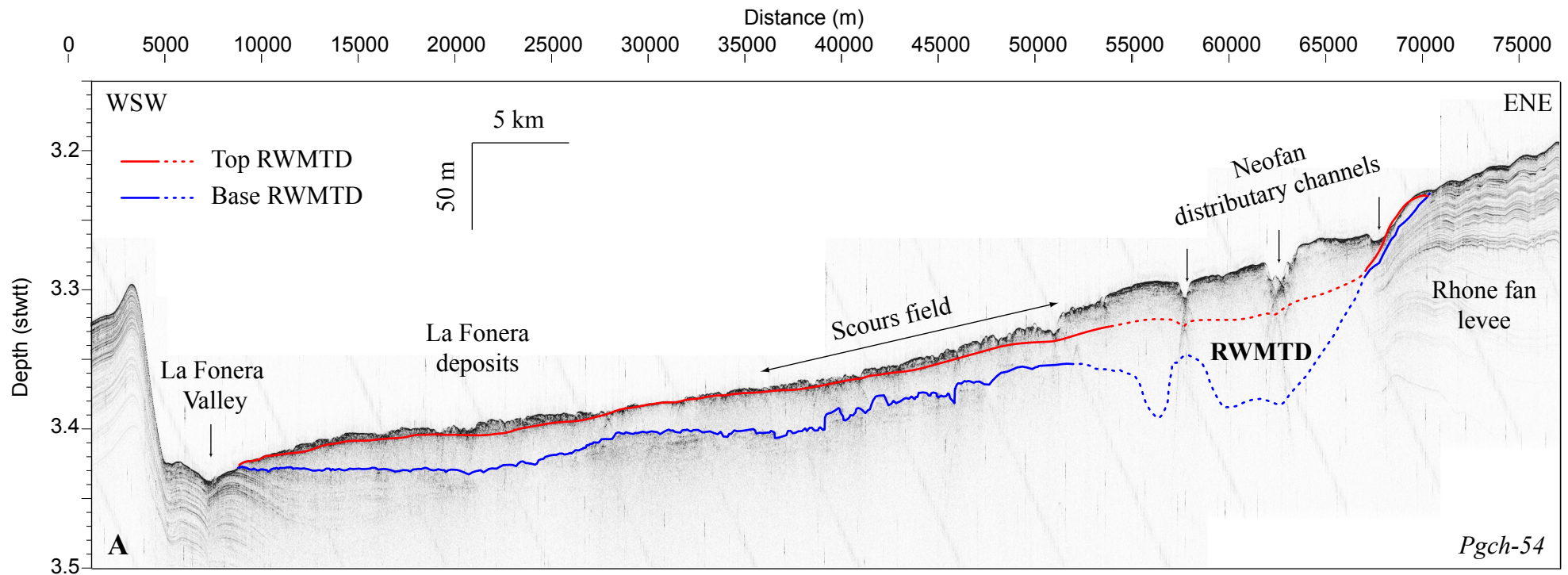


Cal_97-65

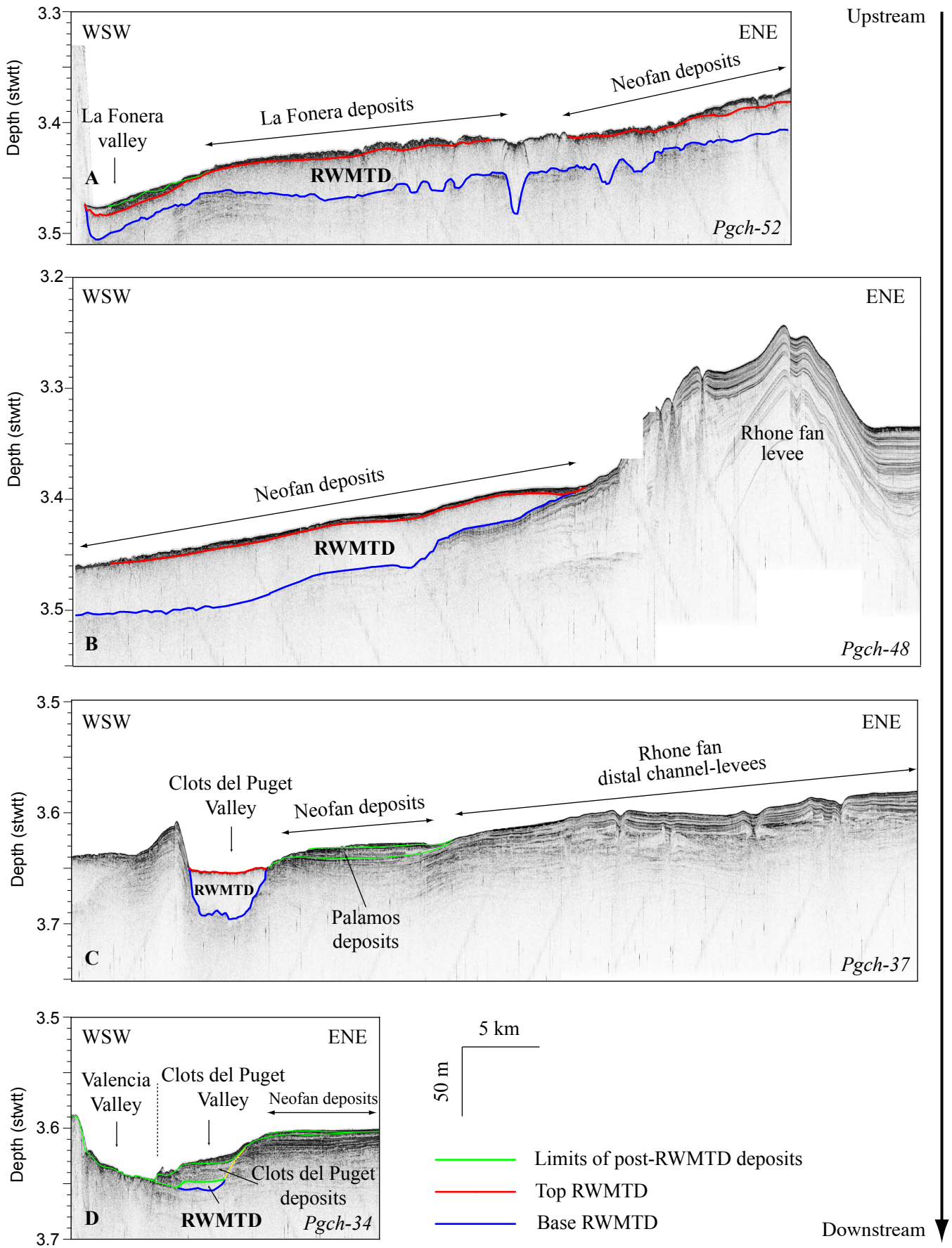
Dennielou et al. RWMTD - Figure 5



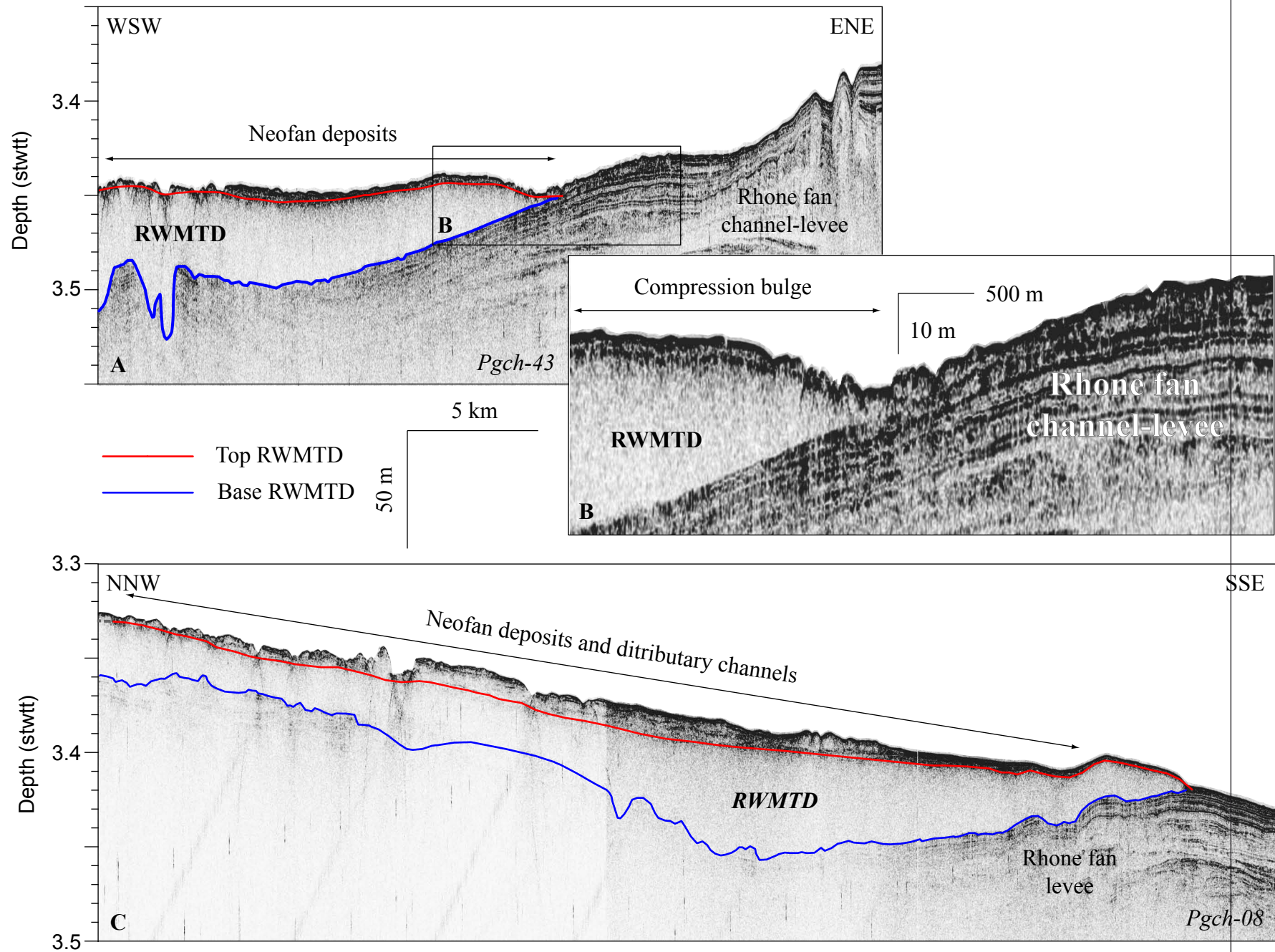
Dennielou et al. RWMTD - Figure 6



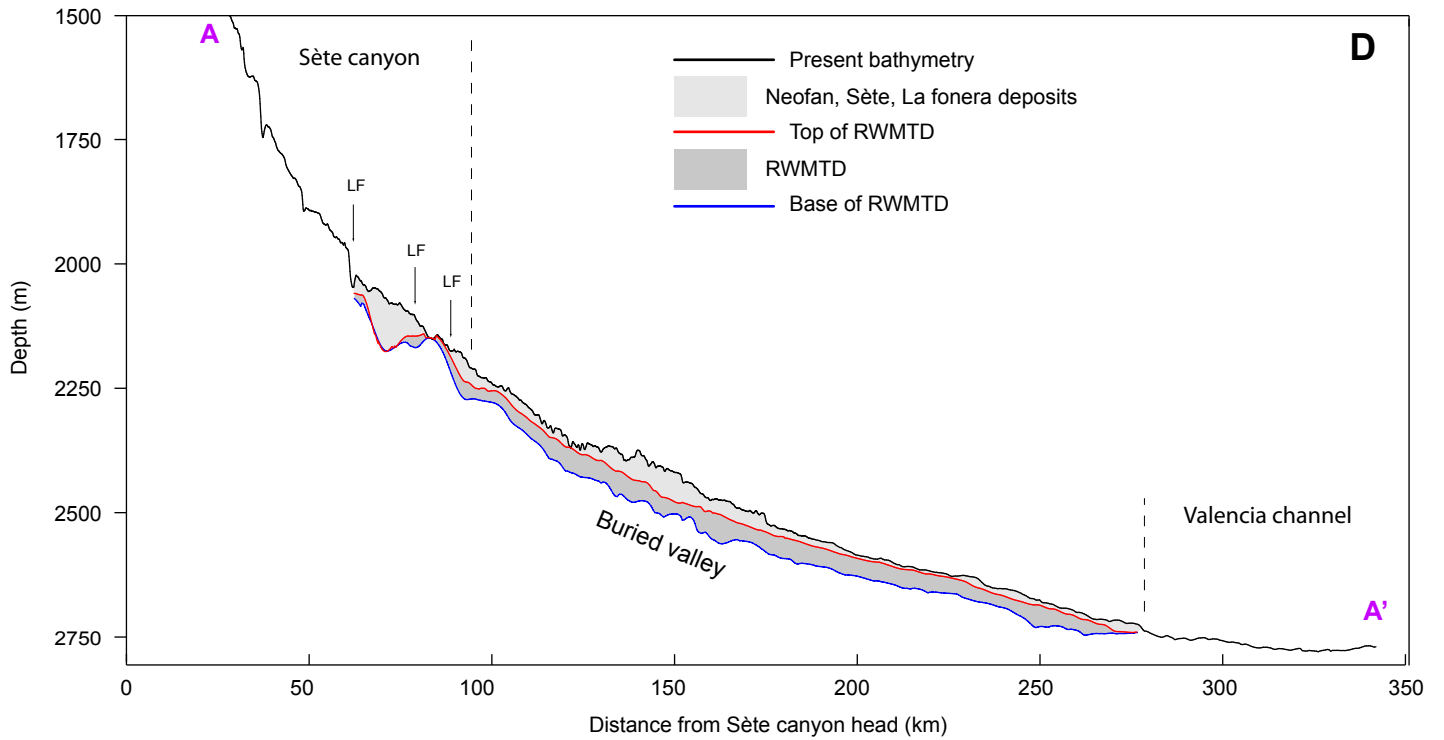
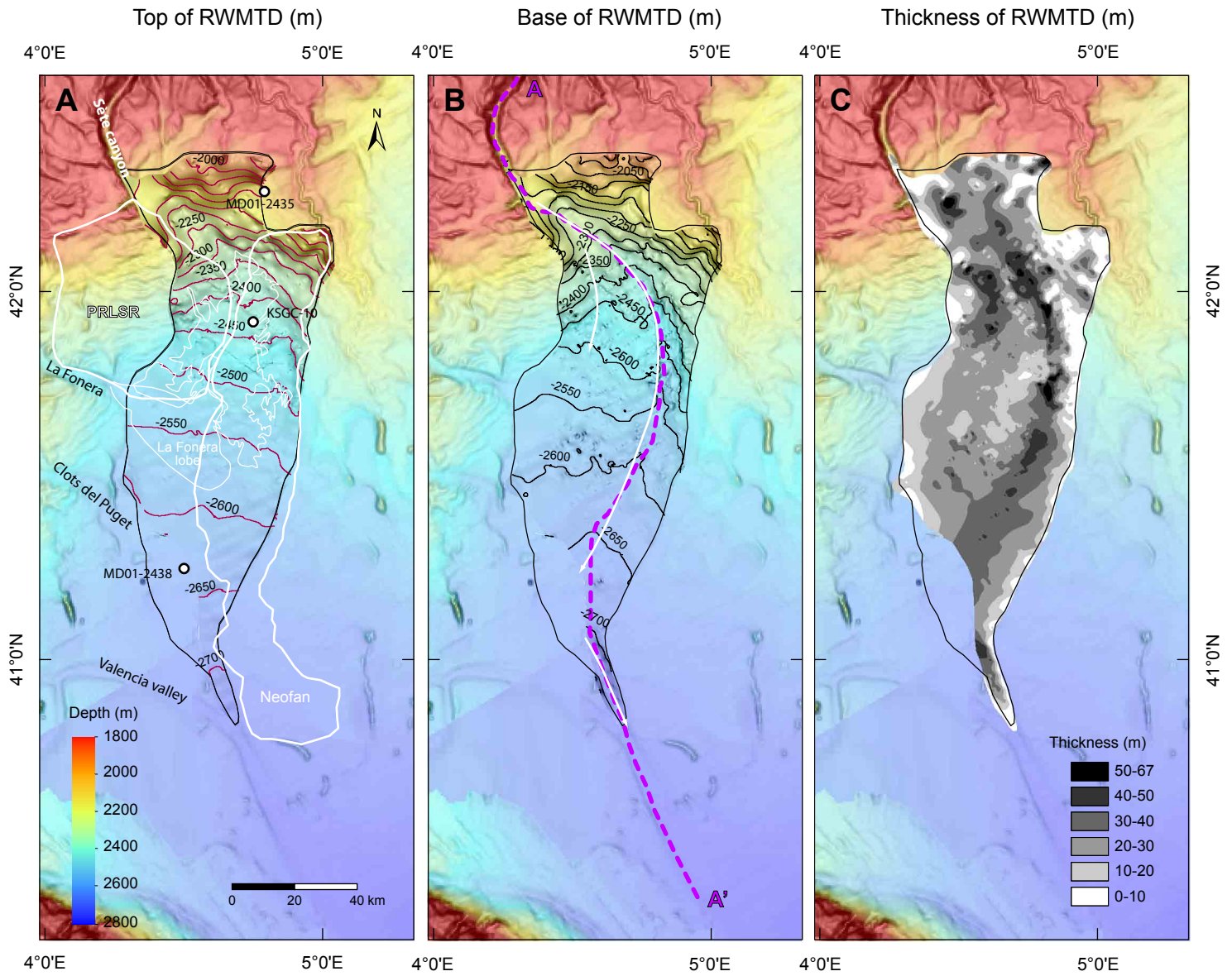
Dennielou et al. RWMTD - Figure 7



Dennielou et al. RWMTD - Figure 8



Dennielou et al. RWMTD - Figure 9

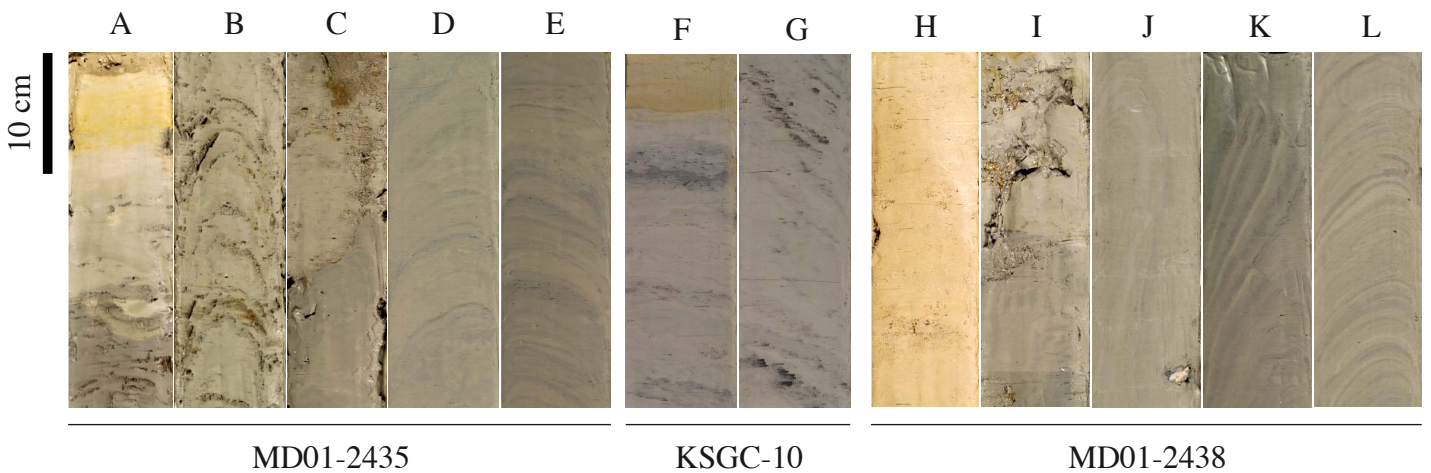
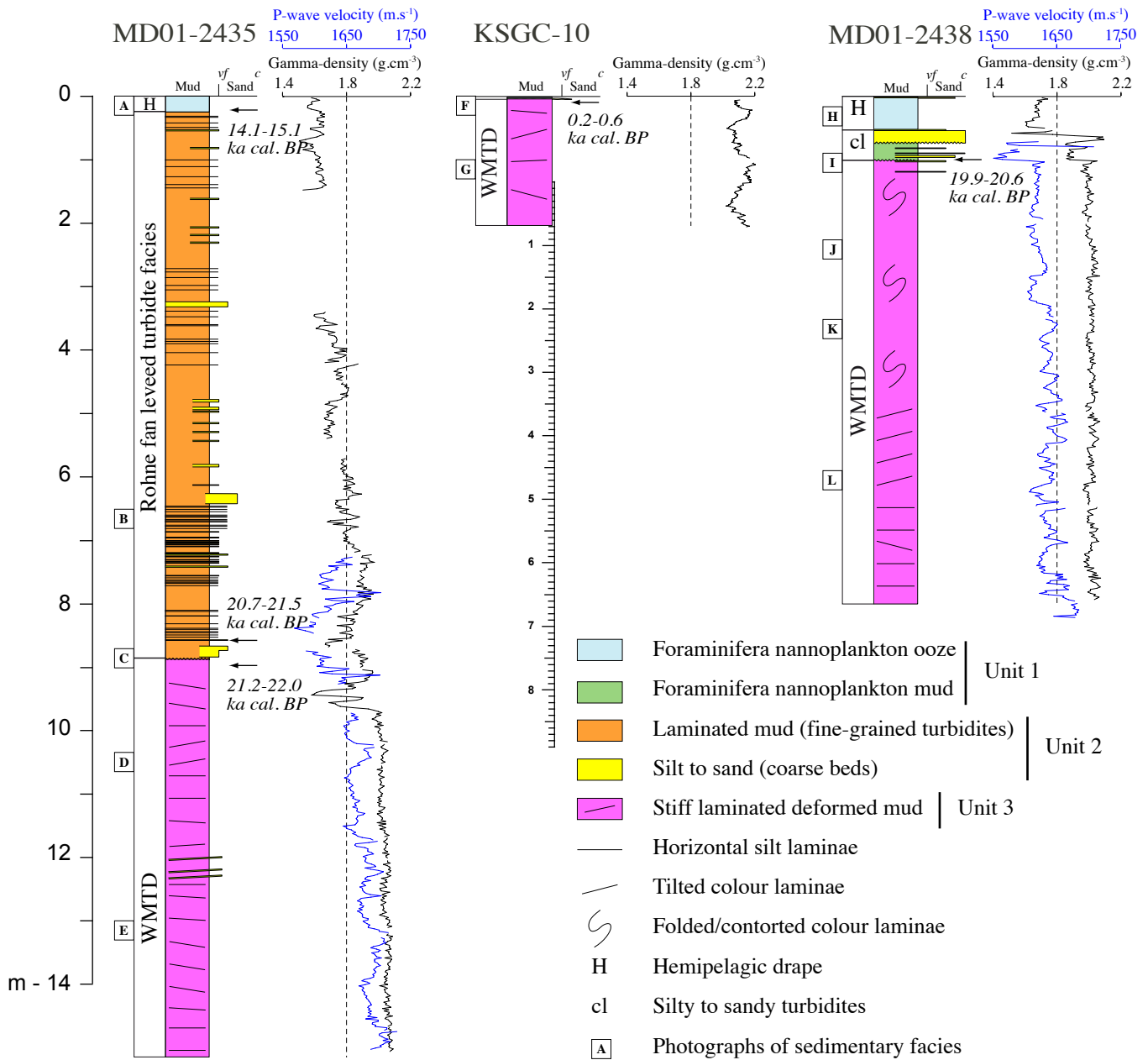


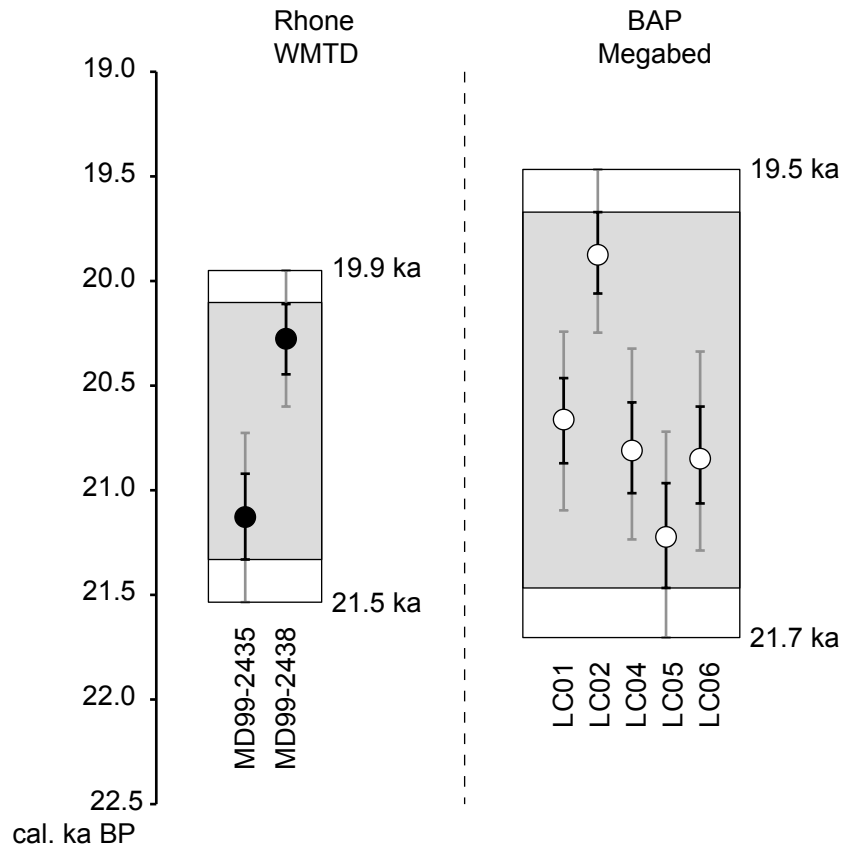
Dennielou et al. RWMTD - Figure 10

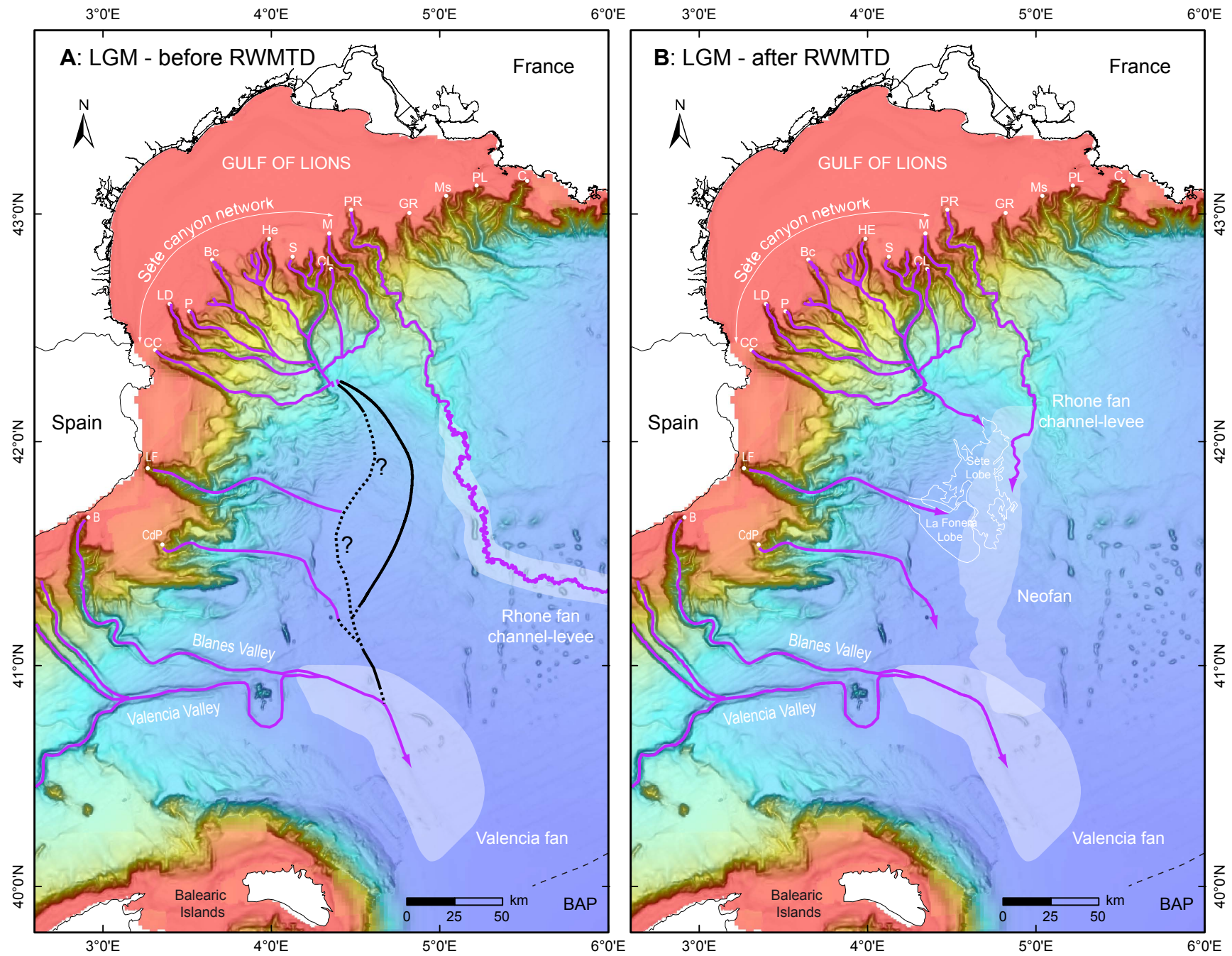
Proximal

Location in the RWMTD

Distal







Dennielou et al. RWMTD - Figure 13